

Review

Future Perspectives on Black Hole Jet Mechanisms: Insights from Next-Generation Observatories and Theoretical Developments

Andre L. B. Ribeiro ^{*} and Nathalia M. N. da Rocha ^{*}

Departamento de Ciências Exatas, Universidade Estadual de Santa Cruz, Rodovia Jorge Amado km 16, Ilhéus 454650-000, Bahia, Brazil

^{*} Correspondence: albr@uesc.br (A.L.B.R.); nmnrocha@uesc.br (N.M.N.d.R.)

Abstract: Black hole jets represent one of the most extreme manifestations of astrophysical processes, linking accretion physics, relativistic magnetohydrodynamics, and large-scale feedback in galaxies and clusters. Despite decades of observational and theoretical work, the mechanisms governing jet launching, collimation, and energy dissipation remain open questions. In this article, we discuss how upcoming facilities such as the Event Horizon Telescope (EHT), the Cherenkov Telescope Array (CTA), the Vera C. Rubin Observatory (LSST), and the Whole Earth Blazar Telescope (WEBT) will provide unprecedented constraints on jet dynamics, variability, and multi-wavelength signatures. Furthermore, we highlight theoretical challenges, including the role of magnetically arrested disks (MADs), plasma microphysics, and general relativistic magnetohydrodynamic (GRMHD) simulations in shaping our understanding of jet formation. By combining high-resolution imaging, time-domain surveys, and advanced simulations, the next decade promises transformative progress in unveiling the physics of black hole jets.

Keywords: jets; black holes; future perspectives; next-generation observatories

1. Introduction

Relativistic jets launched by accreting black holes are among the most energetic and enigmatic phenomena in astrophysics. These collimated outflows, capable of propagating across intergalactic distances, are thought to originate in the immediate vicinity of the event horizon [1–3]. Yet, despite extensive observational campaigns and decades of theoretical modeling, the physical mechanisms underlying jet launching, collimation, and energy dissipation remain unsettled. Addressing these open questions is crucial not only for understanding black hole physics but also for unraveling the impact of active galactic nuclei (AGN) feedback on galaxy formation and evolution [4,5].

The study of black hole jets spans multiple scales and physical regimes, from quantum mechanical processes near the event horizon to large-scale hydrodynamic interactions with the intergalactic medium [6,7]. At the smallest scales, the ergosphere of a rotating black hole provides the energy reservoir that powers these outflows through the Blandford-Znajek mechanism [2]. The efficiency of this process depends critically on the magnetic field configuration threading the black hole, with magnetically arrested disks (MADs) representing the most efficient regime for energy extraction [8,9]. However, the transition from magnetospheric processes to hydrodynamic jet propagation involves complex plasma physics that remains poorly understood [10,11].

Observationally, jets manifest across the electromagnetic spectrum, from radio wavelengths where synchrotron emission traces the bulk motion of relativistic particles to gamma-ray energies where inverse Compton scattering and potentially hadronic processes dominate [12,13].



Academic Editor: Ioana Dutan

Received: 17 November 2025

Revised: 28 December 2025

Accepted: 8 January 2026

Published: 15 January 2026

Citation: . . *Universe* **2026**, *12*, 24.

<https://doi.org/>

Copyright: © 2026 by the authors.

Licensee MDPI, Basel, Switzerland.

This article is an open access article distributed under the terms and conditions of the Creative Commons Attribution (CC BY) license

<https://creativecommons.org/licenses/by/4.0/>.

The multi-wavelength nature of jet emission yields complementary diagnostics of the underlying physics, but also presents challenges in developing unified theoretical frameworks [14]. For instance, the rapid variability observed in blazars at TeV energies implies emission regions smaller than the gravitational radius of the central black hole, challenging our understanding of particle acceleration and energy dissipation in relativistic outflows [15,16].

Recent years have witnessed remarkable advances in jet studies across multiple fronts. The Event Horizon Telescope (EHT) captured horizon-scale imaging of the supermassive black hole M87*, revealing jet-launching structures with unprecedented detail [17–19]. These observations confirmed theoretical predictions about the existence of a bright ring structure surrounding the black hole shadow and established direct evidence for the launching of jets from the immediate vicinity of the event horizon [20]. The asymmetric brightness distribution observed in M87* suggests the presence of ordered magnetic fields and places constraints on the black hole spin and viewing angle [21,22].

High-energy observations from instruments such as Fermi-LAT and H.E.S.S. (High Energy Stereoscopic System) have traced variability in blazar jets down to minute timescales, pointing toward compact emission regions and challenging classical shock-based acceleration models [15,23,24]. These observations reveal that particle acceleration can occur on timescales much shorter than the light-crossing time of the broad-line region, suggesting that acceleration occurs in the jet rather than in external photon fields [25,26]. The detection of orphan flares—gamma-ray flares without corresponding optical counterparts—further supports models where high-energy emission originates in spine-sheath jet structures with different Doppler factors [27,28].

At the same time, general relativistic magnetohydrodynamic (GRMHD) simulations have achieved new levels of sophistication, allowing the exploration of MADs and their efficiency in extracting rotational energy from spinning black holes [9,29,30]. These simulations have revealed that the jet power can exceed the accretion luminosity when the magnetic flux threading the black hole reaches saturation levels [8,31]. The MAD state is characterized by periodic magnetic flux eruptions that modulate the jet power and may explain the observed variability in AGN and X-ray binaries [32,33].

However, many key questions remain unanswered: What determines the efficiency of jet launching? Current models suggest that both black hole spin and magnetic field strength play important roles, but the relative importance of these factors and their interplay with accretion rate remains unclear [34,35]. How is energy dissipated along the jet? While magnetic reconnection, shocks, and turbulence have all been proposed as dissipation mechanisms, their relative contributions and spatial distribution along the jet are not well-determined [36,37]. What role does plasma composition play? The electron-positron versus electron-proton composition of jets affects their radiative signatures and propagation properties, but observational evidence remains limited [38,39]. How do jets couple to their environments? The interaction between jets and their surrounding medium determines the morphology of radio lobes and the efficiency of AGN feedback, but the physics of this coupling involves complex multi-phase processes that are challenging to model [40,41].

The upcoming decade is poised to bring transformative progress in addressing these questions. Several next-generation observatories are expected to open new observational windows into black hole jet physics. The continued development of the EHT will allow multi-frequency and time-resolved imaging of jet-launching regions, probing magnetic field topologies and plasma dynamics at horizon scales [42,43]. Future additions to the EHT array, including space-based telescopes, will extend the baseline coverage and make possible imaging of Sagittarius A*, allowing for comparative studies of jet launching in different environments [44,45].

The Cherenkov Telescope Array (CTA) will revolutionize high-energy astrophysics, enabling population studies of blazars and time-domain analyses of jet flares with unprece-

dented sensitivity [46,47]. CTA’s improved angular resolution and sensitivity will allow detailed studies of jet structure and particle acceleration processes. Its wide field of view and rapid slewing capabilities will be key for follow-up observations of transient events, potentially revealing new classes of jet-powered phenomena [48].

Meanwhile, the Vera C. Rubin Observatory’s Legacy Survey of Space and Time (LSST) will deliver long-term high-cadence monitoring of AGN variability across the sky, offering statistical insights into jet duty cycles and feedback processes [49,50]. LSST’s unprecedented combination of depth, area, and cadence will drive the discovery of rare transients and place statistical limits on jet triggering mechanisms and their dependence on host galaxy properties [51,52].

The Whole Earth Blazar Telescope (WEBT) collaboration exemplifies the power of global, coordinated, multi-wavelength monitoring to probe the extreme and dynamic physics of relativistic jets. Two recent studies — Jorstad et al. [53] and Webb & Sanz [54] — illustrate the extraordinary 2020 WEBT campaign on BL Lacertae to unveil connections across temporal and spatial scales, from hours-long quasi-periodic oscillations (QPOs) to minute-scale micro-variability. WEBT will provide a multi-scale picture where large-scale jet instabilities and small-scale turbulent plasma processes are intrinsically linked.

Together, these facilities promise to bridge the gap between horizon-scale physics and kiloparsec-scale jet propagation. The synergy between high-resolution imaging, time-domain surveys, and multi-wavelength observations will produce a comprehensive view of jet physics across all relevant scales and timescales [55].

Complementing these observational breakthroughs, theoretical models face the challenge of incorporating increasingly complex plasma physics into relativistic frameworks. While GRMHD simulations have been instrumental in revealing the role of large-scale magnetic fields, they often neglect kinetic processes such as particle acceleration and radiative feedback, which are essential for connecting simulations with observations [56,57]. The assumption of ideal Magnetohydrodynamic (MHD) breaks down on scales comparable to the plasma skin depth or gyroradius, where kinetic effects become important for particle acceleration and magnetic reconnection [58,59].

Hybrid approaches that combine fluid dynamics with particle-in-cell (PIC) simulations are emerging as a promising pathway to bridge this gap [60–62]. These methods allow the self-consistent treatment of particle acceleration while maintaining the computational efficiency needed to model large-scale jet propagation. Recent advances in computational techniques, including adaptive mesh refinement and GPU acceleration, are making such hybrid simulations increasingly feasible [63–65].

Furthermore, advances in numerical relativity and high-performance computing will allow simulations to explore parameter spaces relevant for diverse astrophysical systems, from stellar-mass black holes in X-ray binaries to supermassive black holes in AGN [66,67]. The development of new numerical schemes that can handle the extreme dynamic range required to model jets—from the event horizon to kiloparsec scales—remains an active area of research [68,69].

This paper reviews the key opportunities and challenges in the study of black hole jets, focusing on how next-generation instruments and theoretical developments can together transform our understanding of jet physics. We emphasize the multi-scale nature of the problem and the need for interdisciplinary approaches that combine observational astronomy, plasma physics, and computational modeling. Section 2 will outline the main observational perspectives from the EHT, CTA, LSST, and WEBT. Section 3 will discuss jet diversity across different astrophysical systems. Section 4 will cover the current state and future prospects of theoretical models, with an emphasis on GRMHD simulations, plasma microphysics, and jet-environment interactions. Finally, Section 5 will present open questions and future directions in the field.

2. Observational Perspectives

The study of black hole jets requires observations across multiple wavelengths, spatial and time scales. The next generation of astronomical facilities promises to unlock unprecedented insights into jet physics through complementary observational approaches. This section discusses the key capabilities and scientific prospects of three transformative facilities: the Event Horizon Telescope, the Cherenkov Telescope Array, the Vera C. Rubin Observatory, and the Whole Earth Blazar Telescope.

2.1. The Event Horizon Telescope (EHT)

The EHT represents a milestone in high-angular-resolution astronomy, achieving micro-arcsecond imaging through very-long-baseline interferometry at millimeter wavelengths [17,70]. Its first results on M87* demonstrated the feasibility of resolving horizon-scale structures, including the shadow of the black hole and the jet-launching region [17,18]—see Figure 1. These observations revealed the first direct visual evidence of a black hole and confirmed key predictions of general relativity in the strong-field regime [71,72].

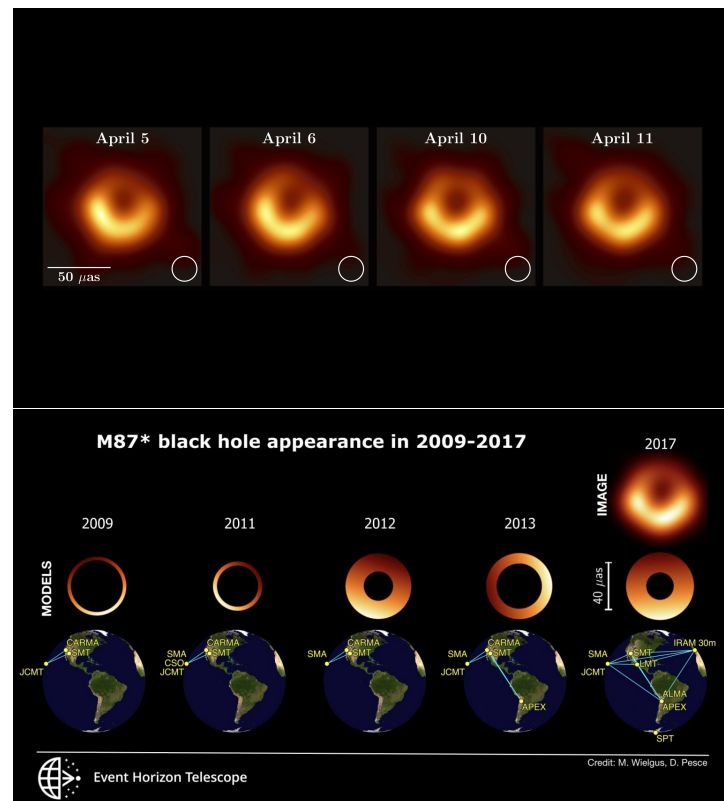


Figure 1. (Top) Observations from the Event Horizon Telescope of the supermassive black hole at the center of the elliptical galaxy M87, for four different days. (Bottom) Snapshots of the M87* black hole appearance, obtained from the EHT array of telescopes in 2009–2017. Where JCMT (James Clerk Maxwell Telescope), CARMA (Combined Array for Research in Millimeter-wave Astronomy), SMT (Heinrich Hertz Submillimeter Telescope), SMA (Submillimeter Array), CSO (Caltech Submillimeter Observatory), APEX (Atacama Pathfinder Experiment), LMT (Large Millimeter Telescope), IRAM (Institute for Radio Astronomy in the Millimetre Range) and SPT (South Pole Telescope). (EHT Collaboration (2019) [73]).

The success of the EHT M87* observations has opened new avenues for studying black hole physics and jet launching mechanisms. The observed asymmetric ring structure imposes restrictions on the black hole spin, the viewing angle, and the magnetic field configuration in the immediate vicinity of the event horizon [21,22]. The brightness asymmetry is consistent with relativistic beaming effects expected from rotating plasma in the

ergosphere, supporting models where jets are launched through the Blandford-Znajek mechanism [74,75].

Future upgrades to the EHT will significantly enhance its scientific capabilities. Expanded frequency coverage, particularly observations at 345 GHz, will provide complementary information about the spectral properties of the emission region and help determine the magnetic field strength through synchrotron spectroscopy [42,76]. The higher frequency observations are less affected by interstellar scattering, potentially revealing finer details of the jet launching region [43,77]. Additionally, 345 GHz observations of Sagittarius A* may be feasible despite the strong scattering in the Galactic center, offering a second target for horizon-scale imaging [78,79].

Increased baseline sensitivity through the addition of new telescopes and improved instrumentation will allow for time-resolved imaging of variability in jet bases [42,43]. This capability is crucial for identifying magnetic flux structures, testing models of MADs, and probing the coupling between black hole spin and jet power [32,33]. The characteristic timescales of variability near the event horizon are expected to be on the order of the gravitational timescale (GM/c^3), which corresponds to minutes for M87* and seconds for Sagittarius A* [80,81]. Detecting and imaging such rapid variability will require coordinated observations with high temporal resolution and sensitivity.

The EHT collaboration is also developing space-based extensions that would dramatically increase the baseline length and angular resolution [44,45]—see Figure 2. A space-based telescope in Earth orbit could deliver baselines exceeding the Earth’s diameter, yielding sub-microarcsecond resolution. Such capabilities would allow detailed imaging of jet collimation and acceleration zones, potentially resolving the transition from magnetospheric to hydrodynamic flow regimes [82,83].

Polarization observations represent another frontier for the EHT [19]. Linear polarization traces the magnetic field structure in the emission region, directly mapping the field geometry responsible for jet launching [84,85]—see Figure 3. Circular polarization can probe the plasma composition and magnetic field strength through Faraday rotation effects [86,87]. The first polarization observations of M87* have already revealed ordered magnetic field structures consistent with theoretical predictions for magnetically dominated jets [19].

Multi-frequency polarization observations will facilitate Faraday rotation measure mapping, delimiting constraints on the electron density and magnetic field strength along the line of sight [88,89]. This technique can distinguish between different models for the plasma composition and magnetic field configuration in the jet launching region. The combination of total intensity and polarization imaging at multiple frequencies will culminate in a comprehensive view of the physical conditions near the event horizon [90,91].

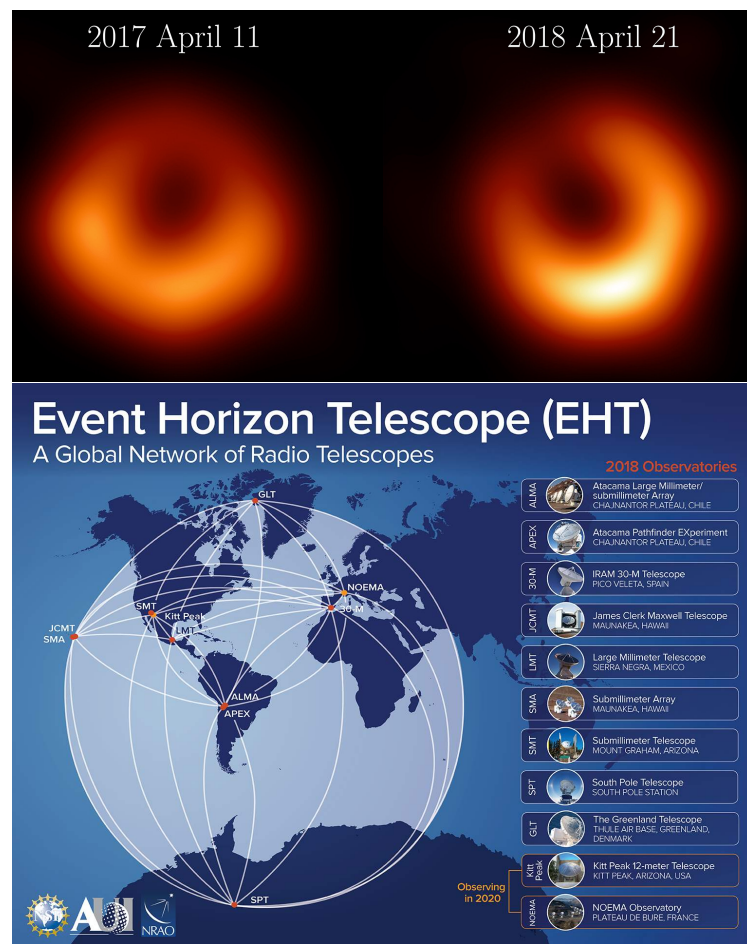


Figure 2. (Top) EHT resolution (EHT collaboration [73]). (Bottom) Diagram of the EHT Network used for the observations in 2017. (Credit: Argonne National Laboratory-NRAO/AUI/NSF).

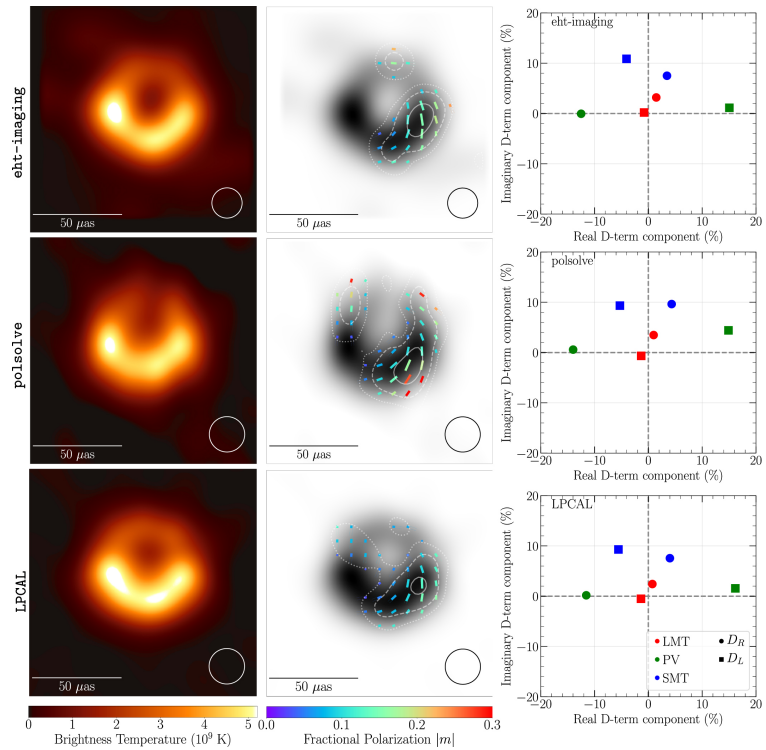


Figure 3. Polarimetric imaging of M87* from 2017 April 11 low-band data. (Left) Total intensity images generated by EHT-imaging, polsolve, and LPCAL. EHT-imaging results are blurred to achieve

a 20 μ as circular Gaussian resolution, matching polslove and LPCAL CLEAN images. (**Middle**) Polarimetric reconstructions following full-array leakage calibration. Total intensity is shown in grayscale background. Polarization ticks represent the Electric Vector Position Angle (EVPA), with their length proportional to the linear polarization intensity magnitude and color indicating fractional linear polarization. Contours illustrate linear polarized intensity at 20, 10, and 5 μ Jy μ as $^{-2}$ (solid, dashed, and dotted, respectively). Regions with Stokes of peak flux density or less than 20% of peak polarized flux density were omitted. A consistent feature across all reconstructions is the predominance of the highest linear polarization fraction and intensity in the southwest part of the ring. (**Right**) Preliminary D-terms for SMT, PV, and LMT, derived through the polarimetric leakage calibration method using EHT-imaging, polslove, and LPCAL. (Credit: EHT collaboration [19]).

2.2. The Cherenkov Telescope Array (CTA)

The CTA will be the most sensitive ground-based gamma-ray observatory to date, covering energies from tens of GeV to hundreds of TeV [46,47]. Its combination of wide sky coverage, excellent temporal resolution, and large collecting area makes it ideal for probing the high-energy emission of blazars and radio galaxies. CTA represents a significant advance over current Cherenkov telescopes, with an order of magnitude improvement in sensitivity and angular resolution [46,48]—see Figure 4.

The enhanced capabilities of CTA will empower several key scientific advances in jet physics. Population studies of blazars will distinguish between leptonic and hadronic emission models via the detailed spectral and temporal information for large samples of sources [14,60,61]. The improved sensitivity will allow detection of fainter sources and extend the redshift range of observable blazars, unveiling insights into the evolution of jet properties with cosmic time [92,93].

CTA will quantify particle acceleration timescales through high-cadence monitoring of blazar flares [94,95]. The rapid variability observed in some blazars implies acceleration timescales shorter than the synchrotron cooling time, requiring efficient acceleration mechanisms such as magnetic reconnection or shock acceleration in highly magnetized plasmas [37,96]. CTA's ability to resolve sub-hour variability will pin down the size and magnetic field strength of acceleration regions [97,98].

The array's improved angular resolution will enable spatial studies of extended gamma-ray emission from radio galaxy jets [99,100]. Current instruments can barely resolve the jet structure in nearby sources like M87, but CTA will unveil detailed maps of gamma-ray emission along jets and in radio lobes [101,102]. These observations will refine models for particle acceleration and energy dissipation in different regions of the jet, from the compact core to the extended lobes [103,104].

CTA's synergy with neutrino detectors such as IceCube may clarify the contribution of relativistic jets to high-energy cosmic messengers [105,106]. Hadronic models for blazar emission predict associated neutrino production through pion decay, but current limits from IceCube are approaching the predictions of some models [107,108]. CTA's improved sensitivity to gamma-ray flares will allow for more precise correlation studies with neutrino detections, potentially establishing the first definitive evidence for hadronic acceleration in jets [109,110].

The wide field of view and rapid slewing capabilities of CTA will ensure follow-up observations of transient events detected by other facilities [46]. Gravitational wave detections of black hole mergers may be associated with jet-powered electromagnetic counterparts, particularly if the merger involves a neutron star [111,112]. CTA's ability to rapidly respond to alerts and conduct deep observations will be fundamental for detecting such rare events [113].

Multi-wavelength coordination with other facilities will maximize the scientific return of CTA observations [14]. Simultaneous observations with radio telescopes can trace

the evolution of synchrotron emission as particles are accelerated to gamma-ray energies [28,114]. X-ray observations furnish complementary information about the electron distribution and magnetic field strength [115,116]. Optical monitoring can characterize external photon fields that contribute to inverse Compton emission [25,117].

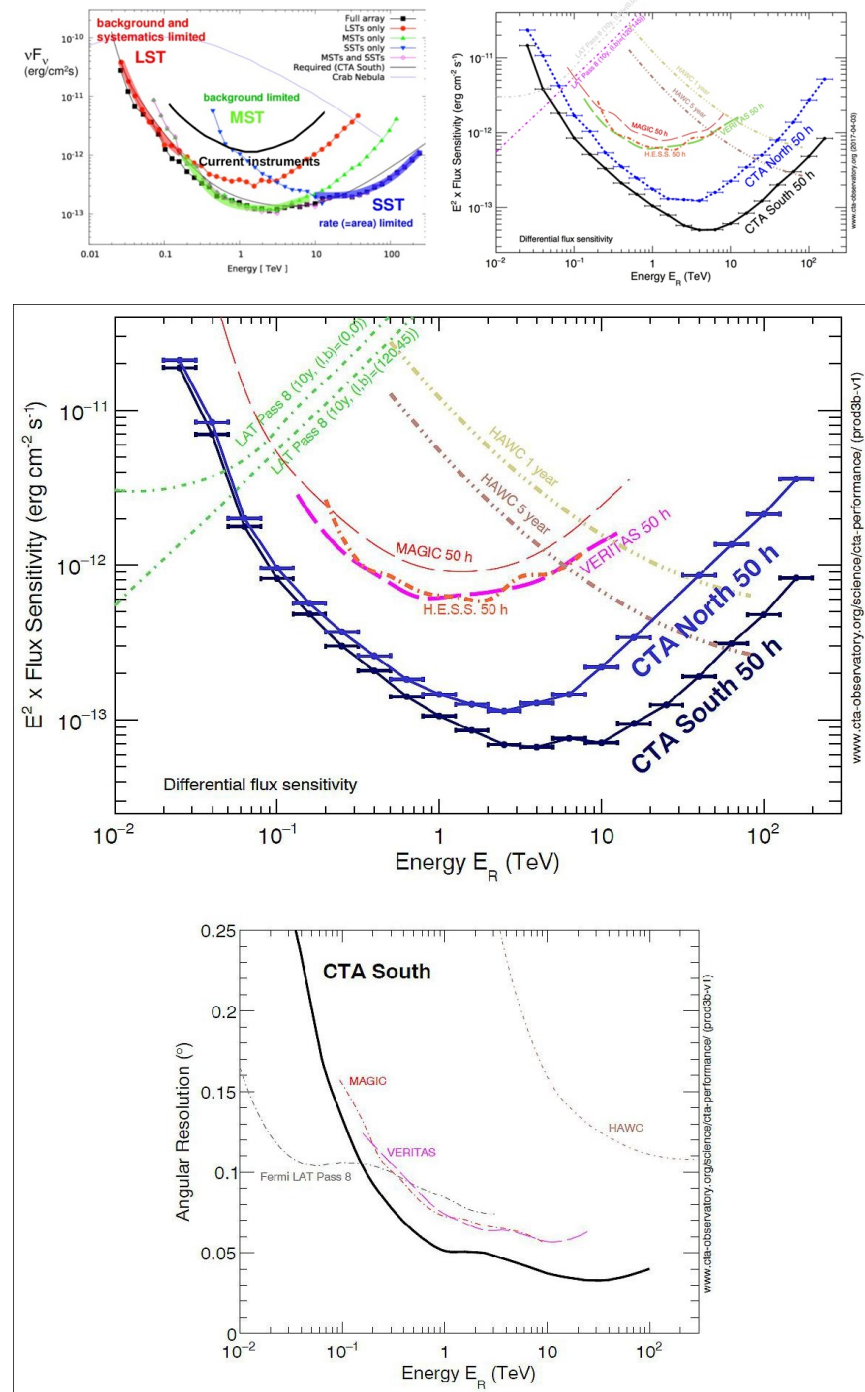


Figure 4. CTA point source sensitivity comparison. **(Top)** Overall sensitivity of the full CTA array (black line, filled squares) against individual telescope types: 4 LSTs (red line, filled circles), 25 MSTs (green line, filled triangles), and 75 SSTs (blue line, upside-down triangles). Current instrument sensitivity for the same observation time is also shown (black line), with expected improvements as analysis algorithms evolve and the final layout is set. **(Bottom)** Differential flux sensitivity for the CTA southern array (black solid line) and northern array (blue dotted line). For context, sensitivities of H.E.S.S., VERITAS, MAGIC (for the same observation time), HAWC (one and five-year observations), and Fermi-LAT (10 years with two diffuse gamma-ray background levels) are included. (Credit: S. Mangano [118] and CTA collaboration-eoPortal [119]).

2.3. The Vera C. Rubin Observatory (LSST)

The LSST will revolutionize time-domain astrophysics by means of its 10-year survey of the southern sky with unprecedented depth and cadence [49,50]—see Figure 5. For AGN and jet studies, LSST will deliver massive statistical samples of optical variability, enabling the study of jet duty cycles, feedback episodes, and correlations with multi-wavelength activity [5,51]. The survey will observe approximately 2×10^{10} galaxies and 1.7×10^{10} stars, thereby producing an unprecedented dataset for statistical studies of AGN variability [49].

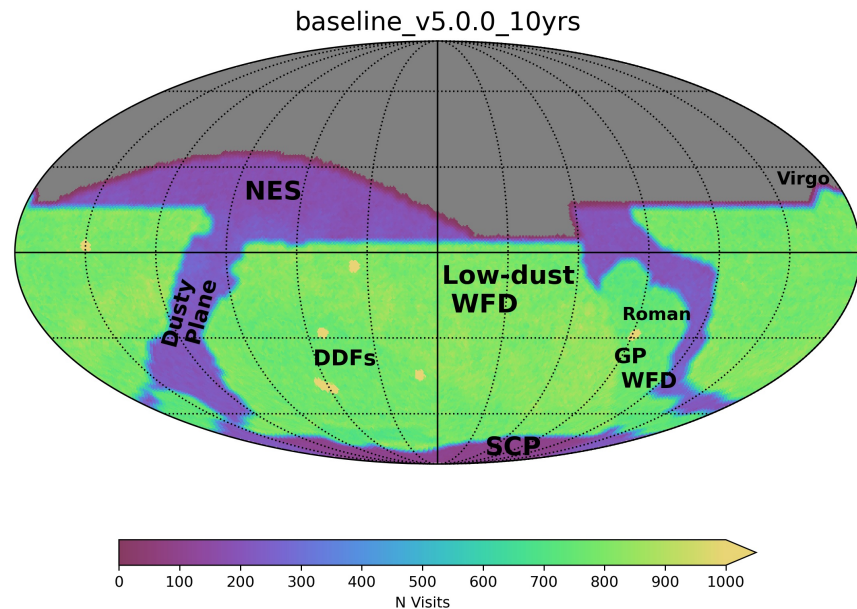


Figure 5. The LSST footprint, illustrating the sky observed over the 10-year survey and the distribution of on-sky visits across the major components of the LSST. Where N Visits (number of visits in the LSST footprint) (Credit: Schwamb et al. 2023 [120]).

LSST’s observing strategy involves repeated observations of the entire visible southern sky every few nights, with deeper observations in selected regions [50]. This approach will generate light curves for millions of AGN with typical cadences of 3–4 days and photometric precision of 1% or better for sources brighter than magnitude 24 [49]. The 10-year baseline will unlock studies of long-term variability patterns and correlations with host galaxy properties [52,121], and pave the way for comprehensive studies of AGN duty cycles and triggering mechanisms [122,123].

Current samples of variable AGN are limited by selection effects and small sample sizes, making it difficult to accurately estimate the fraction of galaxies that host active jets and the timescales for jet activity [124,125]. LSST will furnish unbiased samples of AGN across a wide range of luminosities and redshifts, facilitating statistical studies of jet triggering and its dependence on black hole mass, accretion rate, and host galaxy properties [126,127].

LSST’s ability to capture rare transients, such as tidal disruption events (TDEs) with relativistic jets, will expand our understanding of jet formation beyond the AGN paradigm [128,129]. TDEs represent a unique laboratory for studying jet launching in previously quiescent black holes, potentially revealing the conditions required for jet formation [130,131]. The survey is expected to discover thousands of TDEs, with a subset showing evidence for relativistic outflows through radio and X-ray follow-up observations [132,133].

The survey will also permit studies of AGN feedback through correlations between jet activity and host galaxy properties [4,134]. Optical variability can trace episodes of enhanced accretion and jet activity, which may correlate with star formation rates, galaxy

morphology, and environment [135,136]. Large statistical samples will allow detailed studies of feedback efficiency and its dependence on galaxy mass and environment [137,138].

LSST’s photometric redshift capabilities will make possible studies of AGN evolution across cosmic time [50,139]. The survey will detect AGN out to redshifts exceeding 6, shedding new light on insights into the role of jets in early galaxy formation and the growth of the first supermassive black holes [140,141]. Correlations between jet activity and galaxy assembly can restrict models for AGN feedback in the early universe [142,143].

The survey’s multi-band photometry will yield crude spectral information for millions of AGN, enabling studies of emission line variability and correlations with continuum changes [52,121]. Broad emission lines can respond to continuum variations on timescales of weeks to months, establishing constraints on the size and structure of the broad line region [144,145]. Correlations between line and continuum variability can probe the relationship between accretion disk and jet activity [146,147].

2.4. The Whole Earth Blazar Telescope (WEBT)

Jorstad et al. [53] presents a landmark discovery, rapid (\sim 13-h) quasi-periodic oscillations simultaneously detected in optical flux, optical polarization, and γ -ray flux during a historic outburst of BL Lacertae. The WEBT’s core achievement here is the collection of an unprecedented 16,497 optical photometric and 1285 polarimetric measurements from 37 telescopes worldwide. This dense, continuous sampling is crucial for identifying the transient, short-period QPOs that would be missed by sparse monitoring. The strong, zero-lag correlation between optical and γ -ray fluxes implies a co-spatial origin for the synchrotron (optical) and synchrotron self-Compton (γ -ray) emission regions. This will directly challenge models where these emissions originate in widely separated zones. By synergizing WEBT data with monthly 43 GHz VLBA imaging, the QPO phenomenon is directly tied to a specific physical structure in the jet. The oscillations began as a superluminal knot passed through a quasi-stationary recollimation shock, located \sim 5 pc from the black hole. Also, the multiwavelength QPOs are modeled as a current-driven kink instability in the jet’s helical magnetic field, triggered by the passing shock. This instability creates periodic magnetic reconnection events, accelerating particles and producing the observed correlated flux and polarization oscillations. This model elegantly explains the observed periods and the relationship between flux and polarization variations.

Long-baseline, high-cadence optical monitoring is essential for triggering and interpreting targeted VLBI and high-energy observations. The WEBT will provide the temporal “movie” that gives context to the VLBA “snapshots”, enabling a direct connection between observed variability and parsec-scale jet morphology.

Zooming in from day-long QPOs to minute-hour micro-variability, Webb & Sanz [54] analyzes the intra-night “flickering” in the same 2020 WEBT dataset. The authors isolate 41 well-sampled nights and fit the micro-variability curves with pulses predicted by the “turbulent cell” model. The authors interpret each micro-variability pulse as synchrotron emission from a single turbulent plasma cell—i.e., a localized enhancement in density and magnetic field—being energized as it is crossed by a propagating shock. By deconvolving the observed light curves, they infer the characteristic sizes of these turbulent cells. They probe the micro-physics of the jet plasma—the very medium in which the large-scale kink instability develops—see Figure 6. The inferred cell sizes (order of AU to tens of AU) inform the inner boundary conditions for simulations of jet turbulence and instability growth. The excellent fits of the turbulent cell model (average correlation coefficient of 0.948) to numerous independent nights strongly support the picture that the blazar jet flow is fundamentally turbulent. This turbulence is likely the source of the “random” magnetic field component that dilutes polarization. The WEBT’s unique capability—coordinated,

high-density, long-duration, multi-observer monitoring—has proven indispensable. It will bridge the gap between sporadic space-telescope observations and infrequent VLBI imaging, allowing researchers to connect the dots across time, frequency, and physical scale. The 2020 campaign on BL Lacertae stands as a paradigm for how such collaborations can transform blazar variability from a chaotic curiosity into a powerful diagnostic of relativistic jet physics, from global MHD instabilities down to micro-parsec turbulent plasma structures. the WEBT observations are the ultimate testing ground for the turbulent cell/kink instability model.

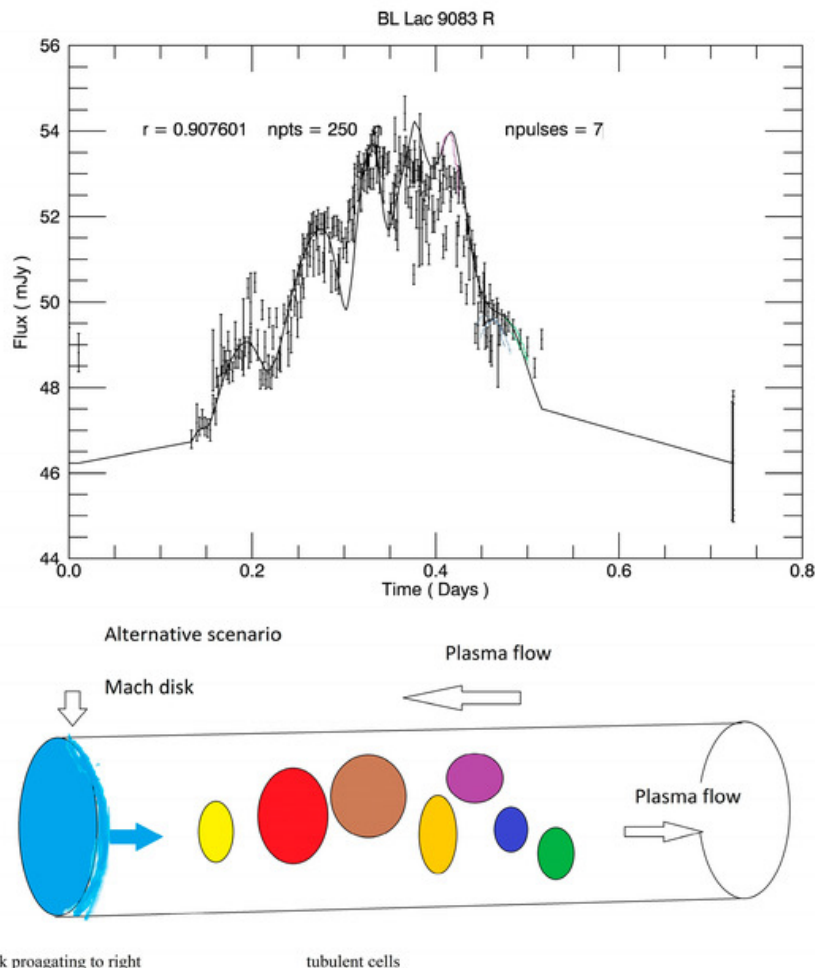


Figure 6. Microvariability curve of BL Lac (top) alongside an illustrative model (bottom) depicting a shock propagating through a turbulent jet. The model demonstrates how the shock triggers radiation pulses from colored density enhancements, which subsequently convolve to produce the observed micro-variability curve, i.e., the illustration shows a blue shock moving from left to right along a jet. As it passes each colored region (density enhancement), it causes a burst of radiation. Adding up all these bursts creates the micro-variability plot shown. (Credit: Webb & Sanz [54]).

2.5. Synergies and Multi-Messenger Astronomy

Before delving into the synergies and multi-messenger astronomy, it is useful to consult Table 1, which presents a comparative overview of the Next-Generation Observatories for Black Hole Jet Studies.

The true power of these facilities lies in their complementarity and the synergies that emerge from coordinated observations. Horizon-scale imaging by the EHT, high-energy light curves from CTA, and long-term monitoring by LSST together provide a multi-scale view of jet physics, from microphysical processes near the event horizon to kiloparsec-

scale propagation [55]. These observational advances, combined with X-ray and neutrino facilities, herald a new era of multi-messenger jet astrophysics [148].

Table 1. Comparative Table of Next-Generation Observatories for Black Hole Jet Studies.

Observatory	Wavelength/Energy Range	Angular Resolution (or Scale)	Sensitivity (Flux Limit)	Sky Coverage/Field of View	Temporal Cadence	Key Contributions to Jet Physics
EHT (Event Horizon Telescope)	Millimeter waves (e.g., 1.3 mm, 0.87 mm)	Horizon scales (μ as)	High (for bright, nearby objects)	Pointed targets (Sgr A*, M87*)	Rapid variability (minutes seconds)	Direct imaging of jet launching regions, magnetic field structures, GR tests
CTA (Cherenkov Telescope Array)	Gamma-rays (GeV-TeV)	Significant angular improvement (arcmin)	\sim 1 order of magnitude better than current	Wide sky coverage, rapid slewing	Blazar variability (sub-hour)	Particle acceleration, emission models, transient event detection, neutrino correlation
LSST (Vera C. Rubin Observatory)	Optical (u, g, r, i, z, y bands)	Wide, for galactic surveys	Down to 27.5 mag	Half sky (Southern Hemisphere)	High cadence (few nights)	AGN variability, jet duty cycles, feedback, TDEs with jets, statistical studies
WEBT (Whole Earth Blazar Telescope)	Multi-wavelength Optical	No intrinsic spatial resolution (point-like)	High (for blazar monitoring)	Selected point targets	Dense, continuous monitoring (h/days)	Rapid variability (QPOs, micro-variability), turbulent plasma physics, kink instability

Coordinated observations between EHT and CTA can directly connect horizon-scale jet launching with high-energy emission [81]. Simultaneous observations during gamma-ray flares can test whether variability originates in the jet launching region or further downstream [28]. The time delays between millimeter and gamma-ray variations can trace the location of gamma-ray emission and the propagation speed of disturbances along the jet [149,150].

LSST's wide-area surveys will identify targets for detailed follow-up with EHT and CTA [51]. The survey will discover new classes of variable AGN and transients that may be associated with jet activity [139]. Rapid alerts from LSST can trigger target-of-opportunity observations with other facilities, thereby allowing multi-wavelength studies of jet flares and outbursts [151].

The WEBT collaboration has provided the most comprehensive, high-cadence, multi-wavelength datasets on blazar variability. When analyzed through the lens of modern theoretical frameworks, these observations do more than just document phenomena—they allow us to deconstruct the physics of relativistic jets across all scales [53,54].

The combination of electromagnetic and gravitational wave observations opens new possibilities for studying jet physics [152]. Black hole mergers detected by LIGO/Virgo may be associated with electromagnetic counterparts powered by jets, particularly in asymmetric mergers or mergers involving neutron stars [111,112]. Multi-messenger observations can determine the efficiency of jet launching in merger events and the role of magnetic fields in the merger process [153,154].

Neutrino astronomy represents another complementary probe of jet physics [106]. High-energy neutrinos can only be produced through hadronic processes, constituting a direct test of hadronic acceleration models in jets [107]. The correlation of neutrino detections with gamma-ray flares observed by CTA can distinguish between leptonic and hadronic emission mechanisms and quantify the cosmic ray acceleration efficiency of jets [109,110].

Future space-based gravitational wave detectors such as LISA (Laser Interferometer Space Antenna) will extend the sensitivity to lower frequencies, potentially detecting the inspiral phase of massive black hole mergers [155]. These events may be associated with electromagnetic precursors as the black holes approach merger, offering advance warning for electromagnetic follow-up observations [156]. The combination of gravitational wave and electromagnetic observations can uncover the role of magnetic fields and jets in the merger process [157].

The development of real-time data processing and alert systems will be decisive for maximizing the scientific return of multi-messenger observations [151]. Rapid identification and characterization of transient events will ensure coordinated follow-up observations across multiple wavelengths and messengers. Machine learning techniques will play an increasingly important role in identifying interesting events in the massive data streams from these facilities [158,159].

3. Jet Diversity Across Astrophysical Systems

The observational capabilities described in the previous section will pave the way for studies of relativistic jets across a wide range of astrophysical systems. While this review focuses primarily on jets from supermassive black holes, the universality of jet physics can be tested by comparing different mass scales and environments. This diversity of jet phenomena demands important tests of theoretical models and motivates the development of unified frameworks that can explain jet physics across all mass scales and environments—see Figure 7.

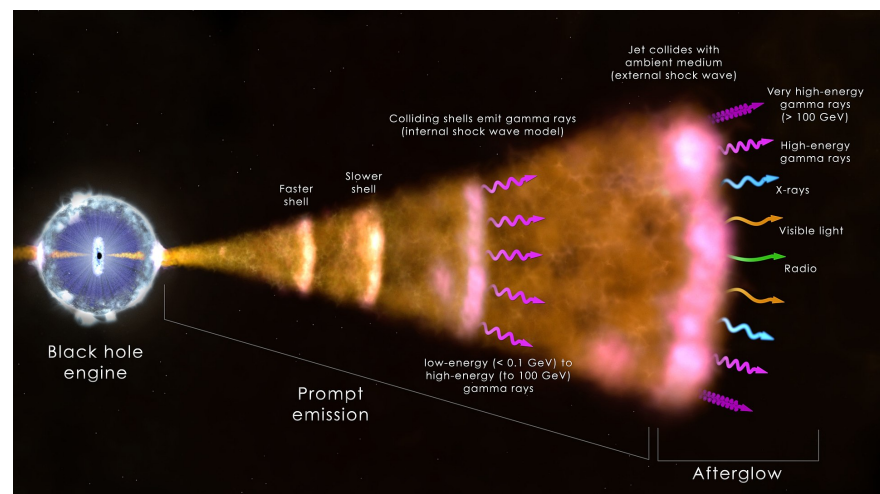


Figure 7. Illustration that shows how the jets of a black hole eject energy ranging from gamma rays to radio frequencies (Credit: NASA/Goddard Research Center/ICRAR).

3.1. Stellar-Mass Black Holes and Microquasars

X-ray binaries containing stellar-mass black holes serve as laboratories for studying jet physics on much shorter timescales than their supermassive counterparts [160,161]. The characteristic variability timescales scale with black hole mass as $t \propto M_{\text{BH}}$, allowing observations of complete outburst cycles and state transitions on human timescales [162,163].

Microquasars such as GRS 1915+105 and Cygnus X-1 exhibit jet launching and quenching on timescales of minutes to hours, unveiling real-time observations of the jet formation process [164,165]. These systems have revealed the existence of discrete jet ejection events and the correlation between accretion state and jet properties [35,166].

The scaling relationships between stellar-mass and supermassive black holes constitute important tests of jet physics [167,168]. The fundamental plane of black hole activity,

relating radio luminosity L_R , X-ray luminosity L_X , and black hole mass M_{BH} , follows the relation:

$$\log L_R = \xi_R \log L_X + \xi_M \log M_{\text{BH}} + \beta \quad (1)$$

where $\xi_R \approx 0.6$, $\xi_M \approx 0.8$, and β is a normalization constant [169,170]. This suggests universal jet launching mechanisms across the mass scale.

3.2. Gamma-Ray Bursts as Extreme Jets

Gamma-ray bursts (GRBs) represent the most extreme manifestation of relativistic jets, with Lorentz factors potentially exceeding $\Gamma > 10^3$ [171,172]. Long GRBs are associated with the collapse of massive stars, while short GRBs likely originate from neutron star mergers [173,174].

The detection of GW170817 and its associated short GRB represented the first direct confirmation of jet formation in neutron star mergers [175,176]. The structured jet model, with a narrow ultra-relativistic core surrounded by a wider, slower component, has emerged as a leading explanation for the observed properties [177,178]. The jet structure can be parameterized as:

$$\Gamma(\theta) = \Gamma_c + (\Gamma_s - \Gamma_c) \left(\frac{\theta}{\theta_c} \right)^{-k} \quad (2)$$

where Γ_c is the core Lorentz factor, Γ_s is the sheath Lorentz factor, θ_c is the core half-opening angle, and k is the power-law index.

GRB jets open a window onto the early universe, as they can be detected out to redshifts exceeding $z > 8$ [179,180]. The use of GRBs as cosmological probes and tracers of star formation in the early universe represents an important application of jet physics [181,182].

3.3. Tidal Disruption Events with Jets

Tidal disruption events (TDEs) occur when a star passes within the tidal radius of a supermassive black hole:

$$r_t = R_* \left(\frac{M_{\text{BH}}}{M_*} \right)^{1/3} \quad (3)$$

where R_* and M_* are the stellar radius and mass, respectively [183,184]. A small fraction of TDEs ($\sim 1\%$) launch relativistic jets, providing insights into jet formation in previously quiescent black holes [185,186].

The jet launching efficiency in TDEs appears to depend on the black hole spin and the magnetic field threading the disrupted stellar material [130,131]. The magnetic flux required for jet formation can be estimated as:

$$\Phi \gtrsim \sqrt{\dot{M}r_g} c \sqrt{4\pi} \quad (4)$$

where \dot{M} is the accretion rate and $r_g = GM_{\text{BH}}/c^2$ is the gravitational radius.

3.4. Scaling Relations and Universal Properties

The diversity of jet-producing systems reveals several universal scaling relations that restrict theoretical models. The jet power scales with accretion rate and black hole mass as:

$$P_{\text{jet}} \propto \dot{M}^\alpha M_{\text{BH}}^\beta \quad (5)$$

where observations suggest $\alpha \approx 1.2\text{--}1.4$ and $\beta \approx 0.8\text{--}1.2$ [34].

The jet opening angle appears to be inversely correlated with jet power:

$$\theta_j \propto P_{\text{jet}}^{-\gamma} \quad (6)$$

with $\gamma \approx 0.1\text{--}0.3$ [187,188]. This relation may reflect the role of magnetic collimation in powerful jets.

The maximum jet Lorentz factor scales with the dimensionless black hole spin parameter a_* as:

$$\Gamma_{\max} \propto \left(\frac{a_*}{1 + \sqrt{1 - a_*^2}} \right)^{1/2} \quad (7)$$

consistent with the Blandford-Znajek mechanism [8,189].

This diversity of jet phenomena across different astrophysical systems compels fundamental tests of theoretical models and motivates the development of unified frameworks that can explain jet physics across all mass scales and environments. The scaling relations observed across different systems suggest that the fundamental physics of jet launching and propagation is universal, despite the vastly different environments in which jets operate.

4. Theoretical Advances and Challenges

The theoretical understanding of black hole jets has advanced significantly over the past decades, driven by improvements in computational capabilities and the development of sophisticated numerical models. However, the multi-scale and multi-physics nature of jet phenomena presents ongoing challenges that require innovative approaches combining fluid dynamics, plasma physics, and general relativity. This section discusses the current state of theoretical models and the key challenges that must be addressed to fully understand jet physics.

4.1. GRMHD Simulations and Jet Launching

General relativistic magnetohydrodynamic (GRMHD) simulations have established the Blandford-Znajek process as a leading mechanism for jet production [2,8,9]. These simulations solve the coupled Einstein-Maxwell-MHD equations in the strong gravitational field near black holes, creating self-consistent models for the extraction of rotational energy from spinning black holes through magnetic field lines threading the ergosphere [190,191].

Recent works demonstrate that MAD configurations can tap black hole spin energy with high efficiency, producing jets that rival accretion luminosity [29,31]. In the MAD state, the magnetic flux threading the black hole reaches saturation levels, leading to efficient energy extraction through the Blandford-Znajek mechanism [192,193]. The jet power in this regime scales approximately as:

$$P_{\text{jet}} \propto a_*^2 \Phi_{\text{BH}}^2 c \quad (8)$$

where a_* is the dimensionless black hole spin, Φ_{BH} is the magnetic flux threading the black hole, and c is the speed of light [189].

The magnetic flux saturation condition can be expressed as:

$$\Phi_{\text{BH}} \lesssim \Phi_{\text{MAD}} \equiv \sqrt{\dot{M}r_g} c \sqrt{4\pi} \quad (9)$$

where \dot{M} is the mass accretion rate and $r_g = GM_{\text{BH}}/c^2$ is the gravitational radius.

GRMHD simulations have revealed several key insights into jet launching mechanisms—see Figure 8. The magnetic field configuration plays a fundamental role in determining jet properties, with large-scale poloidal fields being most efficient for energy extraction [194,195]. The simulations show that jets naturally develop a spine-sheath structure, with a highly relativistic spine surrounded by a slower, more massive sheath [193,196]. This structure arises from the radial dependence of the magnetic field strength and the

varying efficiency of the Blandford-Znajek mechanism across the jet cross-section—see Figure 9.

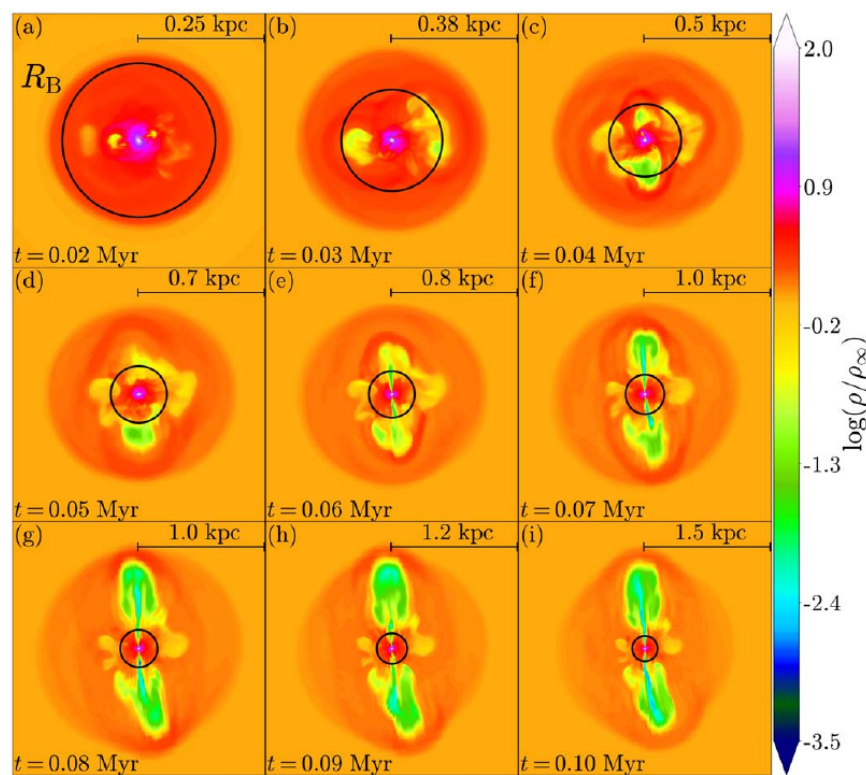


Figure 8. First 3D GRMHD simulation demonstrating the natural emergence of X-shaped radio galaxy morphology from initially axisymmetric conditions. Panels (a–i) display a time sequence of vertical density slices, scaled to M87*, where the color bar depicts the jet density variation. Initially intermittent, low-density jets ($t \lesssim 0.05$ Myr) are frequently disrupted but extend beyond the Bondi radius. As the black hole saturates with magnetic flux and enters a MAD state ($t \sim 0.05$ Myr), jets stabilize, propagate along the z-axis, explaining the rarity of XRGs. This simulation achieves the largest scale separation ($R_B/R_g = 10^3$) to date (Lalakos et al. (2022) [197]).

The simulations also demonstrate that jet power and variability are intimately connected to the accretion flow properties [32,33]. In the MAD state, periodic magnetic flux eruptions occur when the accumulated magnetic flux exceeds the maximum sustainable level [31,198]. These eruptions temporarily reduce the jet power and may explain the observed variability in AGN and X-ray binaries [199,200]. The timescale for these eruptions is typically several times the orbital period at the innermost stable circular orbit:

$$t_{\text{eruption}} \sim (3 - 10) \times \frac{2\pi r_{\text{ISCO}}}{v_{\text{ISCO}}} \quad (10)$$

where r_{ISCO} and v_{ISCO} are the radius and velocity at the innermost stable circular orbit.

However, such simulations often assume idealized plasma conditions, leaving open questions about microphysics and radiative processes [56,57]. The MHD approximation assumes that the plasma can be treated as a conducting fluid, neglecting kinetic effects that become important on small scales [58,59]. The simulations typically use simple prescriptions for the equation of state and neglect radiative cooling, which can significantly affect the dynamics in luminous sources [201,202].

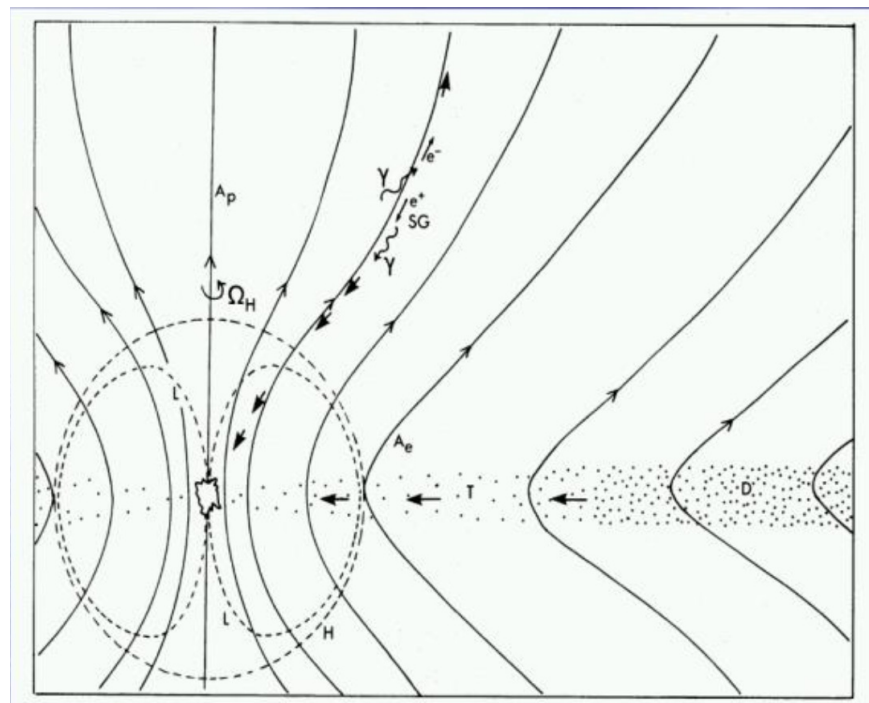


Figure 9. Blandford-Znajek mechanism. (Credit: Blandford-Znajek (1977) [2]).

Current GRMHD codes face several technical challenges that limit their applicability to realistic astrophysical systems [68,69]. The numerical resolution required to capture both the horizon scale physics and the large-scale jet propagation exceeds current computational capabilities. Most simulations are limited to relatively small computational domains, typically extending only a few hundred gravitational radii from the black hole [203,204]. This limitation prevents the study of jet collimation and interaction with the external medium.

The treatment of magnetic field evolution in GRMHD simulations remains challenging due to the need to maintain the divergence-free condition $\nabla \cdot \mathbf{B} = 0$ [205,206]. Various numerical schemes have been developed to address this issue, including constrained transport methods and divergence cleaning techniques [207,208]. However, the accumulation of numerical errors over long simulation times can still lead to unphysical magnetic field configurations.

Recent advances in GRMHD simulations include the development of adaptive mesh refinement techniques that allow higher resolution in regions of interest while maintaining computational efficiency [69,209]. These methods bridge the study of multi-scale phenomena, from the event horizon to the jet propagation region. The implementation of more sophisticated microphysics, including electron heating and cooling processes, is also an active area of development [56,210].

It is also worth mentioning the work of Brian Punsly [211–213] as a refinement of the Blandford-Znajek mechanism, in which he embedded it within a more complete and physically realistic system. Punsly (i) corrected a key dynamical oversight: Magnetic flux dynamics force the strongest field into the ergosphere, not onto the horizon; (ii) identified a more powerful engine: For the fastest-spinning holes, the ergospheric disk wind is the primary power source, not the horizon wind; (iii) proposed a dual-jet structure: This naturally creates a stable, powerful sheath (from ergosphere) plus a variable, energetic core (from horizon); (iv) created a unified diagnostic model: The relative power of these two jets, dictated by black hole spin and accretion history, determines whether we see an OVV quasar, a BL Lac, or a hybrid source. In essence, Punsly's work argued that the Blandford-Znajek jet is the “blazar within the quasar”. It is the inner, violent heart of the

engine, whose relative visibility is controlled by the strength of the more powerful but steadier ergospheric sheath jet that surrounds it. This framework remains a profound and influential way to understand the diversity of relativistic jets.

4.2. Plasma Microphysics and Particle Acceleration

Jets are not simply fluid structures but complex plasma environments where shocks, turbulence, and magnetic reconnection can accelerate particles to ultra-relativistic energies [36,37]. Understanding these microphysical processes is necessary for connecting GRMHD simulations with observational signatures, as the emission properties depend critically on the particle distribution function and magnetic field structure on small scales [214,215].

Particle-in-cell (PIC) simulations have revealed that reconnection can efficiently produce nonthermal power-law particle distributions consistent with observed blazar spectra [61,216]. Magnetic reconnection occurs when oppositely directed magnetic field lines come into contact and reconnect, releasing magnetic energy and accelerating particles [217,218]—see Figure 10. In relativistic plasmas, this process can produce power-law particle distributions with spectral indices similar to those inferred from observations [219,220].

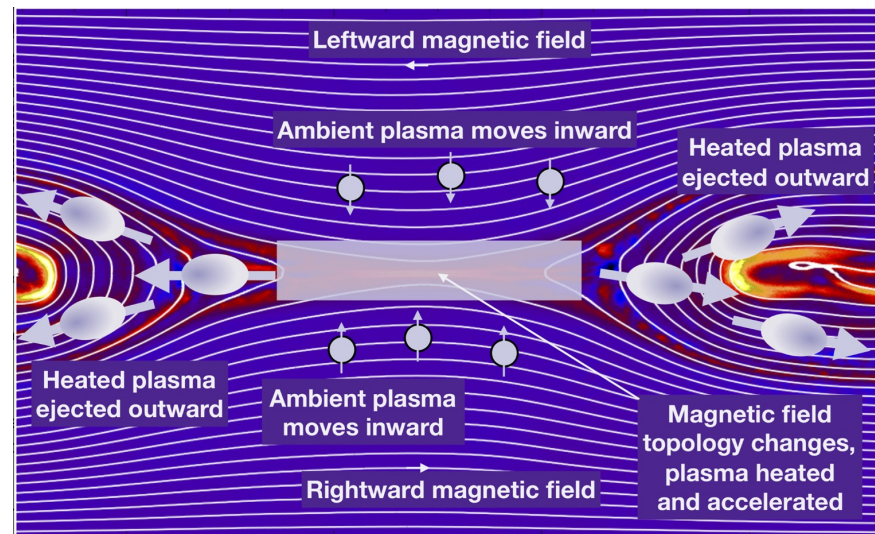


Figure 10. Simplified two-dimensional schematic of magnetic reconnection. Opposing magnetic fields (light blue lines) and ambient plasma (light blue circles) converge into a central diffusion region (shaded box), where reconnection occurs. This process heats and accelerates the plasma, ejecting it into jets (shaded blue ovals) to the left and right. (Credit: Hesse & Cassak (2019) [221]).

PIC simulations of relativistic reconnection show that the acceleration efficiency depends on several factors, including the magnetization parameter:

$$\sigma = \frac{B^2}{4\pi\rho c^2} \quad (11)$$

where B is the magnetic field strength and ρ is the plasma density [37,222]. In highly magnetized plasmas ($\sigma \gg 1$), reconnection can convert a significant fraction of the magnetic energy into particle kinetic energy [223]. The resulting particle distributions typically exhibit power-law tails extending to the highest energies accessible in the simulation [224,225].

The maximum particle energy achievable through magnetic reconnection can be estimated as:

$$\gamma_{\max} \sim \frac{\sigma}{4} \frac{L}{r_L} \quad (12)$$

where L is the system size and $r_L = \gamma mc^2/(eB)$ is the Larmor radius of the particle.

The role of turbulence in particle acceleration has also been investigated through PIC simulations [215,226]. Relativistic turbulence can develop in jets through various instabilities, including the Kelvin-Helmholtz instability at the jet boundary and current-driven instabilities in the jet interior [227,228]. Turbulent acceleration can produce extended particle distributions and may be particularly important in the jet spine where the plasma is highly relativistic [62,229].

The turbulent acceleration rate can be approximated as:

$$\frac{d\gamma}{dt} \sim \frac{c}{L_{\text{turb}}} \left(\frac{\delta B}{B} \right)^2 \gamma \quad (13)$$

where L_{turb} is the turbulent correlation length and $\delta B/B$ is the relative magnetic field fluctuation amplitude.

Shock acceleration remains another important mechanism for particle acceleration in jets [230,231]. Relativistic shocks can form when fast-moving plasma encounters obstacles or when different regions of the jet have different velocities [232,233]. The efficiency of shock acceleration depends on the shock parameters, including the Mach number and the magnetic field orientation [234,235]. Recent PIC simulations have shown that relativistic shocks can produce power-law particle distributions, but the spectral index and maximum energy depend sensitively on the shock parameters [216,233].

For a relativistic shock with Lorentz factor Γ_s , the maximum particle energy is limited by synchrotron losses:

$$\gamma_{\text{max}} \sim \sqrt{\frac{6\pi mc}{\sigma_T B}} \Gamma_s \quad (14)$$

where σ_T is the Thomson scattering cross-section.

Coupling PIC results with GRMHD remains a challenge but is essential for connecting horizon-scale simulations with observable emission [63–65]. The computational requirements for fully kinetic simulations of jets are prohibitive, as the relevant scales range from the plasma skin depth (c/ω_p) to the system size ($\sim 10^6 r_g$) [61]. Hybrid approaches that treat ions as particles and electrons as a fluid, or that use reduced kinetic models, offer promising compromises between accuracy and computational efficiency [236,237].

Recent developments in hybrid PIC-MHD methods attempt to bridge this gap by using PIC simulations to calibrate subgrid models for particle acceleration in MHD simulations [215,238]. These approaches use PIC simulations of local plasma processes to determine acceleration rates and particle distributions, which are then incorporated into global MHD simulations as source terms [239,240]. While promising, these methods require careful validation and may miss important non-local effects.

The plasma composition of jets remains an open question with important implications for particle acceleration and emission [38,39]. Electron-positron plasmas have different acceleration properties compared to electron-proton plasmas, particularly in magnetic reconnection events [241,242]. The pair content of jets can be probed through polarization observations and the detection of gamma-ray absorption features, but current observations provide only weak constraints [243,244].

4.3. Radiative Feedback and Observables

Incorporating radiation into simulations is another frontier that is essential for connecting theoretical models with observational data [56,245]. Radiative transfer models that self-consistently evolve synchrotron, inverse Compton, and hadronic processes are needed to connect theory with data from CTA, LSST, and the EHT [20,246]. This challenge

is compounded by the multi-scale nature of jet emission, which spans from sub-horizon particle dynamics to kiloparsec-scale shocks [14]. To better understand these emission mechanisms, Figure 11 illustrates a typical blazar's Spectral Energy Distribution, clearly showing its synchrotron and inverse Compton components.

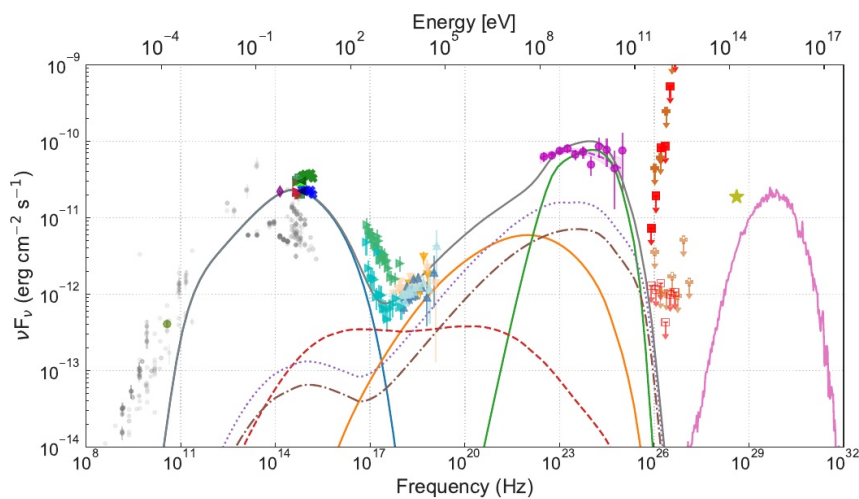


Figure 11. Spectral Energy Distribution (SED) of PKS 0735+178 for December 2021, presented with a model that incorporates radiative contributions from electrons, protons, and an external photon field. For a detailed description of each of the elements presented in the image, check the cited reference. (Credit: VERITAS and HESS collaborations [247]).

The development of general relativistic radiative transfer codes has ushered in more realistic modeling of emission from the vicinity of black holes [248,249]. These codes solve the radiative transfer equation in curved spacetime, accounting for gravitational redshift, light bending, and frame dragging effects [250,251]. The resulting synthetic observations can be directly compared with EHT data, delimiting constraints on the physical conditions in the emission region [90,91].

Synchrotron emission from relativistic electrons in magnetic fields is the dominant radiation mechanism at radio through optical wavelengths [252]. The synchrotron power radiated by an electron with Lorentz factor γ in a magnetic field B is:

$$P_{\text{sync}} = \frac{4}{3} \sigma_T c \beta^2 \gamma^2 \frac{B^2}{8\pi} \quad (15)$$

where $\beta \approx 1$ for relativistic particles.

The emission properties depend on the electron distribution function, magnetic field strength, and geometry [253,254]. GRMHD simulations can predict the magnetic field structure and bulk plasma properties, but the electron distribution must be specified through additional assumptions or microphysical modeling [56,210].

Inverse Compton scattering of low-energy photons by relativistic electrons produces high-energy emission in jets [255,256]. The power radiated through inverse Compton scattering is:

$$P_{\text{IC}} = \frac{4}{3} \sigma_T c \beta^2 \gamma^2 U_{\text{ph}} \quad (16)$$

where U_{ph} is the energy density of the seed photon field.

The seed photons can originate from synchrotron emission within the jet (synchrotron self-Compton, SSC), external radiation fields from the accretion disk or broad line region (external Compton, EC), or the cosmic microwave background [25,257]. The relative

importance of these different seed photon populations depends on the location of the emission region and the external photon field density [26,258].

The ratio of inverse Compton to synchrotron luminosity, known as the Compton dominance parameter, is given by:

$$q = \frac{L_{\text{IC}}}{L_{\text{sync}}} = \frac{U_{\text{ph}}}{U_B} \quad (17)$$

where $U_B = B^2/(8\pi)$ is the magnetic energy density.

Hadronic processes, including proton-proton collisions and photo-meson production, can contribute to high-energy emission and produce neutrinos and cosmic rays [107,259]. These processes require the acceleration of protons to ultra-relativistic energies and sufficient target material or photon fields [14,260]. The efficiency of hadronic acceleration and the resulting emission depend on the plasma composition and the magnetic field structure [108,261].

The threshold energy for photo-meson production is:

$$E_{p,\text{th}} = \frac{m_\pi c^2 (m_\pi + 2m_p)c^2}{4E_{\text{ph}}} \approx \frac{7 \times 10^{16} \text{ eV}}{E_{\text{ph}}/\text{eV}} \quad (18)$$

where m_π and m_p are the pion and proton masses, respectively, and E_{ph} is the target photon energy.

Radiative cooling can significantly affect the dynamics of jets, particularly in luminous sources where the cooling timescale becomes comparable to the dynamical timescale [262,263]. The synchrotron cooling timescale is:

$$t_{\text{sync}} = \frac{6\pi m_e c}{\sigma_T B^2 \gamma} \approx 1.3 \times 10^9 \left(\frac{B}{G} \right)^{-2} \left(\frac{\gamma}{10^4} \right)^{-1} \text{ s} \quad (19)$$

Synchrotron and inverse Compton cooling can reduce the electron energy and modify the emission properties [98,264]. In extreme cases, radiative cooling can affect the jet dynamics through radiation pressure and energy loss [97,265,266].

The implementation of radiative transfer in GRMHD simulations remains computationally challenging due to the need to solve the radiative transfer equation at each grid point and time step [201,202]. Approximate methods, such as the M1 closure or flux-limited diffusion, are often used to reduce the computational cost [267,268]. However, these approximations may not be accurate in optically thin regions or when the radiation field is highly anisotropic [269,270].

Recent advances in GPU computing and machine learning techniques offer new possibilities for accelerating radiative transfer calculations [204,271]. Neural networks can be trained to approximate the radiative transfer solution, potentially reducing the computational cost by orders of magnitude [272,273]. These methods are still in development but show promise for enabling self-consistent radiative GRMHD simulations.

4.4. Jet-Environment Interactions

The interaction between jets and their surrounding environment plays an important role in determining jet morphology and the efficiency of AGN feedback [40,41]. Jets must propagate through the interstellar medium of the host galaxy and potentially through the intracluster medium in galaxy clusters [4,274]. These interactions involve complex multi-phase physics that is challenging to model numerically [275,276].

Hydrodynamic simulations of jet propagation have revealed several key insights into jet-environment interactions [277,278]. Jets can efficiently entrain ambient material,

leading to the formation of cocoons and backflows that can affect the host galaxy [279,280]. The entrainment rate depends on the jet parameters, including the power, opening angle, and density, as well as the properties of the ambient medium [281,282]. These complex interactions, including the formation of characteristic cocoons and lobes, are illustrated in Figure 12.

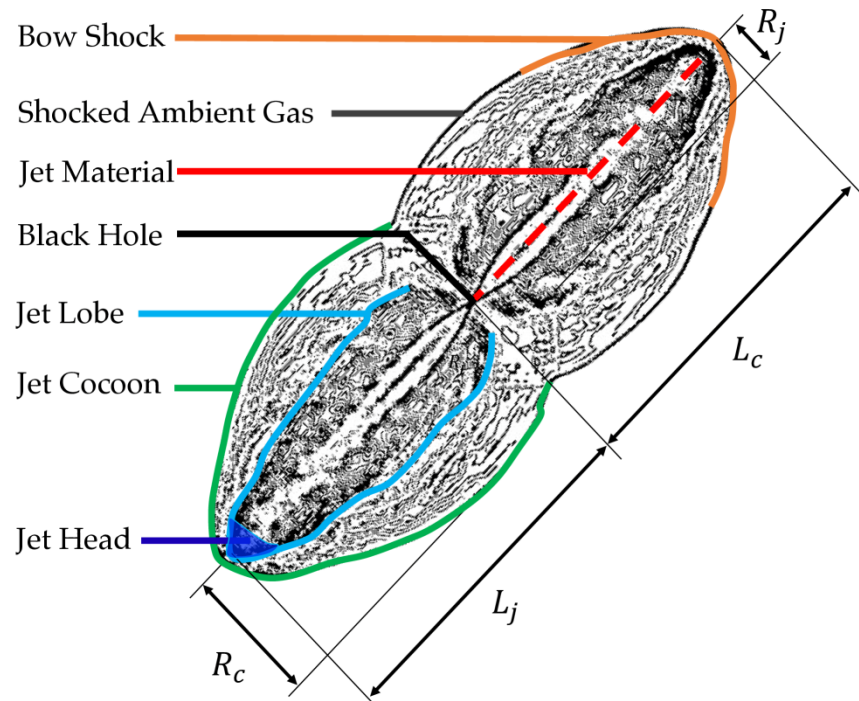


Figure 12. Jet structure derived from a fiducial simulation slice plot. It features a central jet (length L_j , radius R_j) terminating at a jet head, which inflates a lobe of shocked jet material. This lobe is enveloped by a larger cocoon of shocked ambient gas, with a bow shock defining the overall cocoon length (L_c) and radius (R_c) (Credit: GADGET4-OSAKA simulations [283]).

The mass entrainment rate can be estimated as:

$$\dot{M}_{\text{ent}} \sim \rho_{\text{amb}} v_j A_j \left(\frac{\delta v}{v_j} \right) \quad (20)$$

where ρ_{amb} is the ambient density, v_j is the jet velocity, A_j is the jet cross-sectional area, and δv is the velocity difference at the jet boundary.

The Kelvin-Helmholtz instability at the jet boundary can lead to mixing between the jet and ambient material [284,285]. This mixing can reduce the jet velocity and increase the mass loading, affecting the jet propagation and termination [286,287]. The growth rate of the instability depends on the velocity shear and density contrast between the jet and ambient medium [288,289].

The Kelvin-Helmholtz growth rate is approximately:

$$\omega_{\text{KH}} \sim \frac{k \Delta v}{\sqrt{1 + \rho_j / \rho_{\text{amb}}}} \quad (21)$$

where k is the wavenumber, Δv is the velocity difference, and ρ_j and ρ_{amb} are the jet and ambient densities.

Magnetic fields can stabilize jets against disruption by hydrodynamic instabilities [290,291]. Magnetized jets can maintain their collimation over larger distances and are more efficient at transporting energy to large scales [292,293]. However, the magnetic field

configuration can also affect the interaction with the ambient medium, with helical fields potentially enhancing entrainment through magnetic reconnection [294,295].

The formation of shocks in the ambient medium can lead to heating and acceleration of the surrounding gas [296,297]. These shocks can drive outflows and turbulence in the host galaxy, potentially affecting star formation and gas accretion onto the central black hole [298,299]. The efficiency of this feedback depends on the jet power and the properties of the ambient medium [138,300].

The shock heating rate can be expressed as:

$$\dot{E}_{\text{heat}} \sim \frac{P_{\text{jet}}}{V_{\text{cocoon}}} \times f_{\text{coupling}} \quad (22)$$

where V_{cocoon} is the volume of the shocked region and f_{coupling} is the coupling efficiency between jet and ambient medium.

Recent simulations have begun to include more realistic prescriptions for the ambient medium, including multi-phase gas with different temperatures and densities [41,275]. These simulations show that jets can have different effects on different gas phases, potentially leading to complex feedback processes [282,301]. Cold gas clouds can be disrupted or accelerated by jets, while hot gas can be heated and driven out of the galaxy [276,302].

The role of cosmic rays accelerated in jets is another important consideration for jet-environment interactions [303,304]. Cosmic rays can diffuse away from jets and deposit energy in the ambient medium through various processes, including streaming instabilities and hadronic collisions [305,306]. This energy deposition can introduce a distributed heating source that affects the thermal balance of the ambient medium [307,308].

The cosmic ray diffusion coefficient in the ambient medium is typically:

$$D_{\text{CR}} \sim \frac{1}{3} c \lambda_{\text{mfp}} \sim \frac{c r_L}{3} \left(\frac{B}{\delta B} \right)^2 \quad (23)$$

where λ_{mfp} is the mean free path and $\delta B/B$ is the magnetic field fluctuation level.

5. Open Questions and Future Directions

Despite rapid progress in both observational and theoretical studies of black hole jets, several fundamental questions remain unresolved. These open questions span multiple scales and physical regimes, from quantum processes near the event horizon to the large-scale impact of jets on galaxy evolution. Addressing these questions will require coordinated efforts combining next-generation observations, advanced theoretical modeling, and innovative computational techniques.

5.1. Fundamental Physics Questions

5.1.1. Jet Composition and Plasma Physics

One of the most fundamental open questions concerns the composition of relativistic jets [38,39]. Are jets primarily electron-proton or electron-positron dominated? This question has profound implications for jet energetics, particle acceleration mechanisms, and observational signatures. Electron-positron jets would be lighter and potentially more efficient at converting magnetic energy into kinetic energy, while electron-proton jets would carry more mass and could contribute significantly to cosmic ray production [14,309].

The pair-to-proton ratio in jets can be parameterized as:

$$\frac{n_{e^+}}{n_p} \quad (24)$$

where n_{e^+} and n_p are the positron and proton number densities. Current observational constraints suggest $\sim 1\text{--}20$, but with large uncertainties [244].

Current observational evidence on jet composition come primarily from polarization measurements and spectral modeling [243,244]. The degree of linear polarization can trace information about the magnetic field structure and particle distribution, while circular polarization can probe Faraday rotation effects that depend on the plasma composition [310,311]. However, these estimates are often model-dependent and subject to degeneracies between different physical parameters [312,313].

Future polarization observations with the EHT and other facilities may help resolve this question by furnishing detailed maps of the magnetic field structure and Faraday rotation in jet launching regions [19,88]. The detection of gamma-ray absorption features in blazar spectra could also yield limits on the pair content of jets [314,315]. Additionally, neutrino observations may help distinguish between leptonic and hadronic jet models, as only hadronic processes can produce high-energy neutrinos [107,109].

The question of jet composition is closely related to the broader issue of plasma physics in relativistic outflows [58,61]. How do kinetic processes such as magnetic reconnection and turbulence affect the bulk properties of jets? What role do plasma instabilities play in jet collimation and particle acceleration? These questions require detailed kinetic simulations that can capture the full complexity of relativistic plasma physics [59,62].

5.1.2. Acceleration Sites and Mechanisms

What is the dominant mechanism—shocks, turbulence, or reconnection—for accelerating particles to ultra-relativistic energies? This question is central to understanding the high-energy emission from jets and their role as cosmic ray accelerators [37,214]. Different acceleration mechanisms predict different particle distributions, variability timescales, and emission signatures [316,317].

Shock acceleration has been the traditional paradigm for particle acceleration in jets, based on the success of diffusive shock acceleration theory in explaining cosmic ray spectra [318,319]. However, the rapid variability observed in some blazars challenges this paradigm, as it implies acceleration timescales much shorter than those expected from shock acceleration [16,23]. This has led to increased interest in alternative mechanisms such as magnetic reconnection and turbulent acceleration [37,96].

The acceleration timescale for different mechanisms can be compared:

$$t_{\text{shock}} \sim \frac{r_L}{c} \left(\frac{c}{v_s} \right)^2 t_{\text{reconnection}} \sim \frac{L}{c} \frac{1}{\sigma} t_{\text{turbulence}} \sim \frac{L_{\text{turb}}}{c} \left(\frac{B}{\delta B} \right)^2 \quad (25)$$

where v_s is the shock velocity, L is the system size, and L_{turb} is the turbulent correlation length.

Magnetic reconnection can deliver rapid acceleration through the direct conversion of magnetic energy into particle kinetic energy [61,220]. Recent PIC simulations have shown that relativistic reconnection can produce power-law particle distributions with spectral indices consistent with observations [216,225]. However, the efficiency of reconnection in realistic jet environments and its ability to accelerate particles to the highest observed energies remain uncertain [320,321].

Turbulent acceleration through stochastic interactions with magnetic fluctuations offers another possibility for rapid particle acceleration [229,322]. This mechanism can operate continuously throughout the jet and may be particularly important in regions where the plasma is highly magnetized [215,226]. However, the development and maintenance of turbulence in relativistic jets is not well understood, and the efficiency of turbulent acceleration depends on the turbulence spectrum and magnetic field structure [323,324]. Sebastian and

Comisso [325] and Das et al. [326] apply 3D Particle-in-Cell (PIC) simulations to investigate how turbulence in strongly magnetized (high- σ) astrophysical plasmas accelerates particles to non-thermal, high energies. They explore different, recently proposed mechanisms beyond traditional scattering-based theories and highlight complementary mechanisms within the same environment: (i) Mirror acceleration that relies on compressive modes (magnetic pressure); and (ii) Curvature-drift acceleration that relies on shear/torsional modes (magnetic tension).

Future observations with CTA and other high-energy facilities will differentiate between acceleration mechanisms through detailed studies of variability timescales and spectral evolution during flares [47]. The correlation of gamma-ray variability with emission at other wavelengths can help identify the location and mechanism of particle acceleration [28,114]. Multi-wavelength campaigns coordinated with EHT observations may directly connect horizon-scale magnetic field structures with particle acceleration processes [81].

5.2. Jet Dynamics and Structure

5.2.1. Jet Stability and Collimation

How do magnetic instabilities, entrainment, and interaction with the external medium determine jet morphology? Understanding jet stability is necessary for explaining the observed diversity of jet morphologies, from highly collimated pencil beams to wide-angle outflows [40,327]. The stability of jets depends on the balance between magnetic pressure, gas pressure, and external confinement [10,279].

The jet opening angle can be estimated from the balance of forces:

$$\tan \theta_j \sim \sqrt{\frac{P_{\text{gas}} + P_{\text{ext}}}{P_{\text{mag}}}} \quad (26)$$

where P_{gas} , P_{ext} , and P_{mag} are the gas, external, and magnetic pressures, respectively.

Magnetic instabilities such as the current-driven kink mode can disrupt jet collimation and lead to helical distortions [291,295]. The growth rate of these instabilities depends on the magnetic field configuration and the plasma beta parameter [290,293]. While some instabilities can be disruptive, others may play a beneficial role in jet collimation through magnetic pinching effects [328,329].

The kink instability growth rate is approximately:

$$\omega_{\text{kink}} \sim \frac{v_A}{R_j} \sqrt{\frac{k_z R_j}{1 + k_z R_j}} \quad (27)$$

where v_A is the Alfvén velocity, R_j is the jet radius, and k_z is the axial wavenumber.

Entrainment of ambient material can also affect jet stability and propagation [281,282]. The entrainment rate depends on the velocity shear at the jet boundary and the density contrast between the jet and ambient medium [285,286]. Excessive entrainment can lead to jet deceleration and eventual termination, while moderate entrainment may help stabilize the jet through mass loading [276,287].

The external pressure profile also plays a fundamental role in jet collimation [103,280]. Jets propagating through declining pressure profiles will naturally expand and decelerate, while those in increasing pressure environments may be further collimated [277,297]. The pressure profile depends on the host galaxy properties and can vary significantly between different environments [275,282].

Future numerical simulations with improved resolution and physics will help address these questions by following jet evolution over larger spatial and temporal scales [68,69].

The inclusion of realistic ambient medium properties and magnetic field configurations will be crucial for understanding jet stability in different environments [41,303].

5.2.2. Energy Dissipation and Transport

How is energy transported and dissipated along jets from the launching region to the terminal shocks? This question is fundamental to understanding jet energetics and the efficiency of AGN feedback [4,274]. Energy can be transported in various forms, including kinetic energy of the bulk flow, magnetic energy in ordered and turbulent fields, and the energy of relativistic particles [10,196].

The energy flux in different forms can be written as:

$$\dot{E}_{\text{kinetic}} = \frac{1}{2} \dot{M} v^2 \dot{E}_{\text{magnetic}} = \frac{B^2}{4\pi} A v \dot{E}_{\text{Poynting}} = \frac{c}{4\pi} \mathbf{E} \times \mathbf{B} \cdot \hat{\mathbf{n}} A \quad (28)$$

where A is the jet cross-sectional area and $\hat{\mathbf{n}}$ is the normal vector.

The conversion between different energy forms occurs through various dissipation mechanisms [36,37]. Magnetic reconnection can convert magnetic energy into particle kinetic energy and heat [58,61]. Shocks can thermalize kinetic energy and accelerate particles [231,234]. Turbulence can cascade energy from large to small scales where it can be dissipated through various microphysical processes [215,226].

The efficiency of energy transport depends on the jet structure and the presence of instabilities or other dissipation mechanisms [9,193]. Highly magnetized jets may be more efficient at transporting energy to large scales, while kinetically dominated jets may dissipate energy more rapidly through internal shocks and turbulence [11,330].

Observational signatures of energy dissipation come from multi-wavelength studies of jet emission and morphology [103,104]. The radio luminosity of jets quantifies a measure of the energy dissipated through synchrotron emission, while X-ray and gamma-ray observations can probe higher-energy dissipation processes [102,116]. The spatial distribution of emission along jets can also provide information about where energy dissipation occurs [99,100].

5.3. Feedback and Environmental Impact

5.3.1. Feedback Efficiency

How efficiently do jets deposit energy into galactic and cluster environments, and how does this regulate galaxy evolution? This question is central to understanding the role of AGN feedback in galaxy formation and evolution [298,299]. Jets can affect their environment through various mechanisms, including direct heating, driving of outflows, and disruption of gas accretion [138,300].

The feedback efficiency can be quantified as:

$$\eta_{\text{feedback}} = \frac{\dot{E}_{\text{deposited}}}{\dot{E}_{\text{jet}}} \quad (29)$$

where $\dot{E}_{\text{deposited}}$ is the rate of energy deposition in the ambient medium and \dot{E}_{jet} is the jet power.

The efficiency of jet feedback depends on the coupling between jets and the ambient medium [40,41]. This coupling is determined by factors such as the jet power, opening angle, and duty cycle, as well as the properties of the ambient medium including density, temperature, and magnetic field strength [275,301]. The feedback efficiency may also depend on the host galaxy properties and environment [124,125].

Observational evidence for jet feedback comes from studies of galaxy clusters, where jets from central AGN appear to balance radiative cooling of the intracluster medium [4,274].

However, the detailed mechanisms responsible for this balance are not well understood [304]. How do jets maintain the observed temperature and entropy profiles in cluster cores? What role do sound waves, turbulence, and cosmic rays play in distributing energy throughout the cluster? [303,308].

The cooling-heating balance in clusters can be expressed as:

$$\dot{E}_{\text{cooling}} = \Lambda(T)n_e n_H V \approx \dot{E}_{\text{jet}} \times \eta_{\text{feedback}} \quad (30)$$

where $\Lambda(T)$ is the cooling function and n_e, n_H are the electron and hydrogen densities.

Future observations with LSST and other facilities will define statistical bounds on feedback efficiency through studies of large samples of galaxies and clusters [49,50]. The correlation between jet activity and host galaxy properties can reveal the conditions under which feedback is most effective [122,134]. Multi-wavelength observations can trace the impact of jets on different gas phases and provide insights into the physical mechanisms responsible for feedback [282,297].

5.3.2. Duty Cycles and Triggering

What determines the duty cycle of jet activity, and how does it relate to black hole accretion and galaxy mergers? Understanding jet triggering is required for predicting when and where jets will be active and for assessing their cumulative impact on galaxy evolution [123,126].

The duty cycle can be defined as:

$$f_{\text{duty}} = \frac{t_{\text{active}}}{t_{\text{active}} + t_{\text{quiescent}}} \quad (31)$$

where t_{active} and $t_{\text{quiescent}}$ are the durations of active and quiescent phases.

Current models suggest that jet activity may be episodic, with periods of high activity alternating with quiescent phases [35,331]. The duty cycle may depend on factors such as the black hole spin, accretion rate, and magnetic field configuration [9,29]. Galaxy mergers and interactions may also trigger jet activity by driving gas toward the central black hole and enhancing the magnetic flux [141,143].

Observational constraints on duty cycles come from studies of jet morphology and the statistics of AGN activity [124,125]. Double-lobed radio sources suggest episodic activity, while the fraction of galaxies hosting active jets allows us to infer the average duty cycle [40]. However, these inferences are limited by selection effects and the difficulty of measuring jet ages [332].

The jet age can be estimated from the advance speed:

$$t_{\text{jet}} \sim \frac{D_{\text{lobe}}}{v_{\text{advance}}} \sim \frac{D_{\text{lobe}}}{c} \left(\frac{\rho_{\text{jet}}}{\rho_{\text{amb}}} \right)^{1/3} \quad (32)$$

where D_{lobe} is the lobe distance and v_{advance} is the advance velocity.

Future time-domain surveys with LSST will produce unprecedented insights into jet duty cycles through long-term monitoring of AGN variability [52,121]. The survey will detect transitions between active and quiescent states and correlate these with host galaxy properties and environmental factors [139]. The combination of optical monitoring with radio and X-ray observations will assemble a comprehensive view of jet activity cycles [51].

5.4. Multi-Messenger Connections

5.4.1. Cosmic Ray and Neutrino Production

What fraction of high-energy cosmic rays and neutrinos originate in black hole jets? This question connects jet physics to fundamental questions about the origin of cosmic rays and the sources of high-energy neutrinos [107,109]. Jets are among the few astrophysical sources capable of accelerating particles to the highest observed energies [333,334].

The production of ultra-high-energy cosmic rays (UHECRs) requires acceleration to energies exceeding $E > 10^{20}$ eV [334]. This requires either extremely powerful acceleration mechanisms or very large acceleration regions [335]. Jets from AGN are promising candidates for UHECR acceleration, but the acceleration efficiency and maximum energies achievable in realistic jet environments remain uncertain [110,336].

The maximum energy for cosmic ray acceleration in jets is limited by various factors:

$$E_{\max, \text{sync}} \sim \sqrt{\frac{6\pi m_p c^3}{\sigma_T B}} \approx 10^{20} \left(\frac{B}{G} \right)^{-1/2} \text{ eV} \quad (33)$$

$$E_{\max, \text{IC}} \sim \sqrt{\frac{6\pi m_p c^5}{\sigma_T U_{\text{ph}}}} \quad (34)$$

$$E_{\max, \text{escape}} \sim \frac{eBR}{20} \approx 10^{20} \left(\frac{B}{G} \right) \left(\frac{R}{\text{pc}} \right) \text{ eV} \quad (35)$$

Neutrino production in jets requires hadronic processes such as proton-proton collisions or photo-meson production [107,259]. The efficiency of these processes depends on the proton content of jets and the availability of target material or photon fields [108,261]. Current limits from IceCube are beginning to narrow down hadronic models for blazar emission, but definitive detection of neutrinos from jets remains elusive [105,106].

The neutrino production rate through photo-meson interactions is:

$$\dot{N}_\nu \sim f_\pi \times n_p \times \sigma_{p\gamma} \times c \times n_\gamma \times V \quad (36)$$

where $f_\pi \approx 0.2$ is the fraction of proton energy transferred to pions, $\sigma_{p\gamma}$ is the photo-meson cross-section, and n_p, n_γ are the proton and photon densities.

Future observations with next-generation neutrino detectors such as IceCube-Gen2 and KM3NeT will provide improved sensitivity to neutrino emission from jets [337], however recent observations may already represent landmark discoveries in multi-messenger astrophysics, connecting cosmic-ray acceleration with extreme phenomena in the universe. These observations are: (i) the brightest gamma-ray burst (GRB) ever recorded, GRB 221009A [338,339]; (ii) the highest-energy neutrino event KM3-230213A, from NGC 1068 (a Seyfert galaxy that shows a steady neutrino flux from a decade of data) [340]; and (iii) the Telescope Array observation of the Amaterasu particle, an ultra-high-energy cosmic ray with an estimated energy of ~ 244 EeV (2.44×10^{20} eV) [341] that may have originated from NGC 1068 – the same nearby Seyfert galaxy identified by IceCube as a source of high-energy neutrinos, although [342] proposes the blazar PKS 1717+177 as a candidate source for the Amaterasu particle.

Furthermore, the correlation of neutrino detections with gamma-ray flares observed by CTA can help distinguish between leptonic and hadronic emission models [47]. The detection of neutrinos from individual sources would constitute definitive evidence for hadronic acceleration in jets [110]. UHECRs remain one of the most intriguing puzzles in astroparticle physics. While recent data have provided strong hints about their origins—particularly pointing to nearby starburst galaxies—definitive identification of sources and accelera-

tion mechanisms will require more data, better composition measurements, and deeper multi-messenger correlations [343].

5.4.2. Gravitational Wave Associations

How do jets relate to gravitational wave sources, particularly black hole mergers and neutron star disruptions? The detection of gravitational waves has opened a new window into extreme astrophysical phenomena and may unveil insights into jet formation in previously unexplored regimes [152,344].

Black hole mergers detected by LIGO/Virgo may be associated with electromagnetic counterparts powered by jets, particularly in asymmetric mergers or mergers involving neutron stars [111,112]. The efficiency of jet launching in merger events depends on the magnetic field configuration and the properties of any surrounding material [153,154]. Numerical relativity simulations are beginning to explore these scenarios, but observational data remains limited [157].

The jet power from black hole mergers can be estimated as:

$$P_{\text{jet}} \sim \frac{a_*^2 \Phi^2 c}{6\pi M^2} \sim 10^{52} \left(\frac{a_*}{0.9} \right)^2 \left(\frac{\Phi}{10^{30} \text{ G cm}^2} \right)^2 \left(\frac{M}{60 M_{\odot}} \right)^{-2} \text{ erg s}^{-1} \quad (37)$$

Neutron star mergers, such as GW170817, can produce jets that power gamma-ray bursts and kilonovae [175,176]. The properties of these jets and their interaction with merger ejecta offer insights into jet formation in neutron star environments [178,345]. The detection of gravitational waves from neutron star mergers triggers advance warning for electromagnetic follow-up observations [113].

Future gravitational wave detectors with improved sensitivity will detect more merger events and potentially reveal new classes of sources [346]. Space-based detectors such as LISA will extend the sensitivity to lower frequencies, potentially detecting the inspiral phase of massive black hole mergers [155]. These observations may reveal electromagnetic precursors associated with jet activity before merger [156].

The gravitational wave strain from massive black hole mergers at cosmological distances is:

$$h \sim \frac{GM_{\text{chirp}}}{c^2 d} \left(\frac{GM_{\text{chirp}} \pi f}{c^3} \right)^{2/3} \quad (38)$$

where $M_{\text{chirp}} = (M_1 M_2)^{3/5} / (M_1 + M_2)^{1/5}$ is the chirp mass and f is the gravitational wave frequency.

5.5. Technological and Methodological Advances

5.5.1. Computational Challenges

The study of black hole jets requires computational methods that can handle the extreme dynamic range and multi-physics nature of the problem [68,69]. Current simulations are limited by computational resources and numerical methods, preventing the study of jets across all relevant scales simultaneously [203,204].

The computational challenge can be quantified by the range of scales:

$$\frac{L_{\text{max}}}{L_{\text{min}}} \sim \frac{10^6 r_g}{c/\omega_p} \sim 10^{12} \left(\frac{M_{\text{BH}}}{10^9 M_{\odot}} \right) \left(\frac{n}{10^6 \text{ cm}^{-3}} \right)^{1/2} \quad (39)$$

Future advances in high-performance computing, including exascale systems and specialized architectures such as GPUs, will enable more detailed simulations of jet physics [63,64,209]. The development of adaptive mesh refinement and multi-scale methods will allow simulations to capture both the small-scale microphysics and large-scale

dynamics [69]. Machine learning techniques may also play an increasingly important role in accelerating simulations and identifying patterns in complex datasets [158,271].

The integration of different physical processes, including general relativity, magnetohydrodynamics, kinetic plasma physics, and radiative transfer, remains a major challenge [56,210]. Hybrid methods that combine different approaches for different regions or scales offer a promising path forward [62,65]. The development of standardized simulation codes and comparison projects will help validate these methods and identify their limitations [347].

5.5.2. Data Analysis and Interpretation

The next generation of observational facilities will produce unprecedented amounts of data, requiring new methods for analysis and interpretation [50,151]. Machine learning techniques will be essential for identifying interesting events in large datasets and for extracting physical parameters from complex observations [158,159].

The data volume from LSST alone is estimated as:

$$V_{\text{data}} \sim 20 \text{ TB night}^{-1} \times 3650 \text{ nights} \sim 70 \text{ PB} \quad (40)$$

The development of standardized data formats and analysis pipelines will facilitate comparison between different observations and theoretical models [43]. Virtual observatory tools will allow for researchers to access and analyze data from multiple facilities simultaneously [139]. The integration of observational data with theoretical models through Bayesian inference and other statistical methods will impose more robust parameter estimation [72].

The interpretation of multi-messenger observations requires sophisticated models that can predict the correlated signals across different messengers [148]. The development of such models and the statistical methods needed to analyze multi-messenger data will be decisive for maximizing the scientific return of future observations [113].

6. Conclusions

Black hole jets remain one of the grand challenges of modern astrophysics, encompassing fundamental physics from quantum mechanics to general relativity and spanning scales from the event horizon to intergalactic distances. The upcoming synergy of next-generation facilities—EHT, CTA, LSST, and WEBT—together with theoretical advances in GRMHD, kinetic plasma simulations, and radiative transfer, promises a transformative leap forward in our understanding.

The multi-scale nature of jet physics requires interdisciplinary approaches that combine observational astronomy, theoretical physics, and computational modeling [55]. The questions outlined in this review span multiple areas of physics and astrophysics, from the fundamental nature of spacetime near black holes to the large-scale structure and evolution of the universe. Addressing these questions will require unprecedented coordination between different observational facilities and theoretical approaches.

The Event Horizon Telescope has already demonstrated the power of horizon-scale imaging in exploring jet launching mechanisms and black hole properties [17,19]. Future developments, including multi-frequency observations, time-resolved imaging, and space-based extensions, will supply even more detailed insights into the physics near the event horizon [42,43]. The combination of total intensity and polarization observations will reveal the magnetic field structure responsible for jet launching and collimation.

The Cherenkov Telescope Array will revolutionize our understanding of particle acceleration in jets through unprecedented sensitivity to high-energy gamma rays [47]. Its ability to detect rapid variability and resolve extended emission will constrain acceleration

mechanisms and energy dissipation processes. The synergy with neutrino detectors may finally resolve the question of hadronic versus leptonic acceleration in jets [107,109].

The Vera C. Rubin Observatory will unlock statistical insights into jet duty cycles, triggering mechanisms, and feedback efficiency through long-term monitoring of millions of AGN [49,50]. Its discovery of rare transients will expand our understanding of jet formation beyond the traditional AGN paradigm. The correlation of optical variability with multi-wavelength observations will reveal the connection between accretion and jet activity.

The WEBT has moved blazar studies from phenomenology to quantitative astrophysics. It demonstrates that optical and multifrequency monitoring is not merely light curve collection, but a powerful tool for “remote sensing” of relativistic plasma. Webb [265] turbulent cell model provided the theoretical language to interpret the small-scale structures. The 2020 WEBT campaign on BL Lacertae provided the perfect, data-rich “laboratory” to apply this model at the micro-scale Webb & Sanz [54] and, simultaneously, to discover how those turbulent structures coexist with and modify large-scale magnetohydrodynamic instabilities [53]. The WEBT collaboration will provide the definitive evidence for turbulence and instability as the twin engines of blazar variability.

On the theoretical front, the development of more sophisticated numerical models that can bridge the gap between horizon-scale physics and large-scale propagation remains a key challenge [68,69]. The incorporation of kinetic plasma physics into GRMHD simulations will be necessary for connecting theory with observations [61,62]. Advances in computational techniques and high-performance computing will permit more realistic simulations that can capture the full complexity of jet physics.

The study of black hole jets also exemplifies the growing importance of multi-messenger astronomy [148]. The combination of electromagnetic observations, gravitational waves, and neutrinos represents complementary probes of jet physics that can break degeneracies inherent in single-messenger observations. Future detections of gravitational waves from black hole mergers may reveal new pathways for jet formation and illuminate insights into the role of magnetic fields in extreme gravitational environments.

By connecting microphysics near the event horizon with the macroscopic impact of feedback on galaxies and clusters, the study of black hole jets stands poised to illuminate fundamental processes of energy transport and cosmic evolution. The next decade will likely see major breakthroughs in our understanding of these remarkable phenomena, with implications extending far beyond the study of black holes themselves.

The success of this endeavor will require continued investment in observational facilities, theoretical research, and computational infrastructure [55]. It will also require fostering collaboration between different communities and disciplines, from high-energy astrophysics to galaxy formation and cosmology. The study of black hole jets exemplifies the interconnected nature of modern astrophysics and the power of combining multiple observational and theoretical approaches to address fundamental questions about the universe.

As we stand on the threshold of a new era in jet astrophysics, the convergence of revolutionary observational capabilities and sophisticated theoretical models promises to finally unlock the secrets of these cosmic accelerators. The journey from the event horizon to the cosmic web, mediated by relativistic jets, represents one of nature’s most extraordinary phenomena and continues to challenge our understanding of the fundamental laws of physics.

Author Contributions: A.L.B.R. was specifically responsible for the Conceptualization, Supervision, funding acquisition and writing—original draft preparation of the work. N.M.N.d.R. undertook the tasks of Project administration, writing—review and editing, and Visualization. All authors have read and agreed to the published version of the manuscript.

Funding: This research was funded by CNPq (Conselho Nacional de Desenvolvimento Científico e Tecnológico), grant number 316317/2021-7.

Data Availability Statement: No new data were created or analyzed in this study. Data sharing is not applicable to this article.

Acknowledgments: The authors thank the referees for very helpful suggestions. N.M.N.d.R. thanks the support of PROBOL-UESC. A.L.B.R. also acknowledges the support from the CNPq (Conselho Nacional de Desenvolvimento Científico e Tecnológico) under Grant No. 404160/2025-5 (CNPq/MCTI Call No. 44/2024—Universal).

Conflicts of Interest: The authors declare no conflicts of interest.

Abbreviations

The following abbreviations are used in this manuscript:

EHT	Event Horizon Telescope
CTA	Cherenkov Telescope Array
LSST	Vera C. Rubin Observatory's Legacy Survey of Space and Time
MADs	Magnetically Arrested Disks
GRMHD	General Relativistic Magnetohydrodynamic
AGN	Active Galactic Nuclei
H.E.S.S.	High Energy Stereoscopic System
MHD	Magnetohydrodynamic
PIC	particle-in-cell
TDEs	Tidal Disruption Events
LISA	Laser Interferometer Space Antenna
GRBs	Gamma-ray Bursts
SSC	Synchrotron Self-Compton
EC	External Compton
GPU	Graphics Processing Unit
UHECRs	Ultra-High-Energy Cosmic Rays
IceCube	Cubic-Kilometer Cherenkov Particle Detector
KM3NeT	Cubic Kilometre Neutrino Telescope
LIGO	Laser Interferometer Gravitational-Wave Observatory
WEBT	Whole Earth Blazar Telescope
JCMT	James Clerk Maxwell Telescope
CARMA	Combined Array for Research in Millimeter-wave Astronomy
SMT	Heinrich Hertz Submillimeter Telescope
SMA	Submillimeter Array
CSO	Caltech Submillimeter Observatory
APEX	Atacama Pathfinder Experiment
LMT	Large Millimeter Telescope
IRAM	Institute for Radio Astronomy in the Millimetre Range
SPT	South Pole Telescope

References

1. Blandford, R.D.; Payne, D.G. Hydromagnetic flows from accretion discs and the production of radio jets. *Mon. Not. R. Astron. Soc.* **1982**, *199*, 883–903. [[CrossRef](#)]
2. Blandford, R.D.; Znajek, R.L. Electromagnetic extraction of energy from Kerr black holes. *Mon. Not. R. Astron. Soc.* **1977**, *179*, 433–456. [[CrossRef](#)]
3. Meier, D.L. *Black Hole Astrophysics: The Engine Paradigm*, 1st ed.; Springer Science & Business Media: Berlin/Heidelberg, Germany, 2012; p. 596.
4. Fabian, A.C. Observational Evidence of Active Galactic Nuclei Feedback. *Annu. Rev. Astron. Astrophys.* **2012**, *50*, 455–489. [[CrossRef](#)]

5. Heckman, T.M.; Best, P.N. The Coevolution of Galaxies and Supermassive Black Holes: Insights from Surveys of the Contemporary Universe. *Annu. Rev. Astron. Astrophys.* **2014**, *52*, 589–660. [\[CrossRef\]](#)
6. Begelman, M.C.; Fabian, A.C.; Rees, M.J. Implications of very rapid TeV variability in blazars. *Mon. Not. R. Astron. Soc. Lett.* **2008**, *384*, L19–L23. [\[CrossRef\]](#)
7. Krolik, J.H. *Active Galactic Nuclei. From the Central Black Hole to the Galactic Environment*; Princeton University Press: Princeton, NJ, USA, 1999.
8. McKinney, J.C.; Tchekhovskoy, A.; Blandford, R.D. General relativistic magnetohydrodynamic simulations of magnetically choked accretion flows around black holes. *Astrophys. J.* **2012**, *423*, 3083–3117. [\[CrossRef\]](#)
9. Tchekhovskoy, A.; Narayan, R.; McKinney, J.C. Black hole spin and the radio loud/quiet dichotomy of active galactic nuclei. *Astrophys. J.* **2010**, *711*, 50. [\[CrossRef\]](#)
10. Komissarov, S.S. Magnetic acceleration of relativistic active galactic nucleus jets. *Mon. Not. R. Astron. Soc.* **2007**, *380*, 51–70. [\[CrossRef\]](#)
11. Lyubarsky, Y. Asymptotic structure of poynting-dominated jets. *Astrophys. J.* **2009**, *698*, 1570. [\[CrossRef\]](#)
12. Degrange, B.; Fontaine, G. Introduction to high-energy gamma-ray astronomy. *Comptes Rendus. Phys. Gamma-Ray Astron./Astron. Des. Rayons Gamma* **2015**, *16*, 587–599. [\[CrossRef\]](#)
13. Urry, C.M.; Padovani, P. Unified schemes for radio-loud active galactic nuclei. *Publ. Astron. Soc. Pac.* **1995**, *107*, 803. [\[CrossRef\]](#)
14. Böttcher, M.; Reimer, A.; Sweeney, K.; Prakash, A. Leptonic and hadronic modeling of Fermi-detected blazars. *Astrophys. J.* **2013**, *768*, 54. [\[CrossRef\]](#)
15. Ackermann, M.; Anantua, R.; Asano, K.; Baldini, L.; Barbiellini, G.; Bastieri, D.; Becerra Gonzalez, J.; Bellazzini, R.; Bissaldi, E.; Blandford, R.D.; et al. Minute-timescale >100 MeV γ -ray variability during the giant outburst of 3C 279 observed by Fermi-LAT. *Astrophys. J.* **2016**, *824*, L20. [\[CrossRef\]](#)
16. Aharonian, F.; Akhperjanian, A.G.; Bazer-Bachi, A.R.; Behera, B.; Beilicke, M.; Benbow, W.; Berge, D.; Bernlöhr, K.; Boisson, C.; Bolz, O.; et al. An exceptional very high energy gamma-ray flare of PKS 2155-304. *Astrophys. J. Lett.* **2007**, *664*, L71. [\[CrossRef\]](#)
17. Event Horizon Telescope Collaboration. First M87 Event Horizon Telescope Results. I. The Shadow of the Supermassive Black Hole. *Astrophys. J. Lett.* **2019**, *875*, L1. [\[CrossRef\]](#)
18. Event Horizon Telescope Collaboration. First M87 Event Horizon Telescope Results. V. Physical Origin of the Asymmetric Ring. *Astrophys. J. Lett.* **2019**, *875*, L5. [\[CrossRef\]](#)
19. Event Horizon Telescope Collaboration. First M87 Event Horizon Telescope Results. VII. Polarization of the Ring. *Astrophys. J. Lett.* **2021**, *910*, L12. [\[CrossRef\]](#)
20. Dexter, J.; Jiménez-Rosales, A.; Ressler, S.M.; Tchekhovskoy, A.; Bauböck, M.; de Zeeuw, P.T.; Eisenhauer, F.; von Fellenberg, S.; Gao, F.; Genzel, R.; et al. A parameter survey of Sgr A* radiative models from GRMHD simulations with self-consistent electron heating. *Mon. Not. R. Astron. Soc.* **2020**, *494*, 4168–4186. [\[CrossRef\]](#)
21. Event Horizon Telescope Collaboration. First M87 Event Horizon Telescope Results. VI. The Shadow and Mass of the Central Black Hole. *Astrophys. J. Lett.* **2019**, *875*, L6. [\[CrossRef\]](#)
22. Narayan, R.; Johnson, M.D.; Gammie, C.F. The Shadow of a Spherically Accreting Black Hole. *Astrophys. J. Lett.* **2019**, *885*, L33. [\[CrossRef\]](#)
23. Albert, J.; Aliu, E.; Anderhub, H.; Antoranz, P.; Armada, A.; Baixeras, C.; Barrio, J.A.; Bartko, H.; Bastieri, D.; Becker, J.K.; et al. Variable very high energy γ -ray emission from Markarian 501. *Astrophys. J.* **2007**, *669*, 862. [\[CrossRef\]](#)
24. HESS Collaboration. Characterizing the gamma-ray long-term variability of PKS 2155-304 with H.E.S.S. and Fermi-LAT. *Astron. Astrophys.* **2017**, *598*, A39.
25. Ghisellini, G.; Tavecchio, F.; Foschini, L.; Ghirlanda, G.; Maraschi, L.; Celotti, A. General physical properties of bright Fermi blazars. *Mon. Not. R. Astron. Soc.* **2010**, *402*, 497–518. [\[CrossRef\]](#)
26. Tavecchio, F.; Ghisellini, G.; Foschini, L.; Bonnoli, G.; Ghirlanda, G.; Coppi, P. The intergalactic magnetic field constrained by Fermi/Large Area Telescope observations of the TeV blazar 1ES 0229+200. *Mon. Not. R. Astron. Soc. Lett.* **2010**, *406*, L70–L74. [\[CrossRef\]](#)
27. Jorstad, S.G.; Marscher, A.P.; Lister, M.L.; Stirling, A.M.; Cawthorne, T.V.; Gear, W.K.; Gómez, J.L.; Stevens, J.A.; Smith, P.S.; Forster, J.R.; et al. Polarimetric Observations of 15 Active Galactic Nuclei at High Frequencies: Jet Kinematics from Bimonthly Monitoring with the Very Long Baseline Array. *Astrophys. J.* **2005**, *130*, 1418. [\[CrossRef\]](#)
28. Marscher, A.P.; Jorstad, S.G.; Larionov, V.M.; Aller, M.F.; Aller, H.D.; Lähteenmäki, A.; Agudo, I.; Smith, P.S.; Gurwell, M.; Hagen-Thorn, V.A.; et al. Probing the inner jet of the quasar PKS 1510-089 with multi-waveband monitoring during strong gamma-ray activity. *Astrophys. J. Lett.* **2010**, *710*, L126. [\[CrossRef\]](#)
29. Narayan, R.; Chael, A.; Chatterjee, K.; Ricarte, A.; Curd, B. Jets in magnetically arrested hot accretion flows: Geometry, power, and black hole spin-down. *Mon. Not. R. Astron. Soc.* **2022**, *511*, 3795–3813. [\[CrossRef\]](#)
30. White, C.J.; Stone, J.M.; Quataert, E. A Resolution Study of Magnetically Arrested Disk. *Astrophys. J.* **2019**, *874*, 168. [\[CrossRef\]](#)

31. Tchekhovskoy, A.; Narayan, R.; McKinney, J.C. Magnetohydrodynamic simulations of gamma-ray burst jets: Beyond the progenitor star. *New Astron.* **2010**, *15*, 749–754. [\[CrossRef\]](#)

32. Liska, M.; Hesp, C.; Tchekhovskoy, A.; Ingram, A.; van der Klis, M.; Markoff, S. Formation of precessing jets by tilted black hole discs in 3D general relativistic MHD simulations. *Mon. Not. R. Astron. Soc. Lett.* **2017**, *31*, L81–L85. [\[CrossRef\]](#)

33. Ripperda, B.; Liska, M.; Chatterjee, K.; Musoke, G.; Philippov, A.A.; Markoff, S.B.; Tchekhovskoy, A.; Younsi, Z. Black Hole Flares: Ejection of Accreted Magnetic Flux through 3D Plasmoid-mediated Reconnection. *Astrophys. J. Lett.* **2022**, *924*, L32. [\[CrossRef\]](#)

34. Nemmen, R.S.; Georganopoulos, M.; Guiriec, S.; Meyer, E.T.; Gehrels, N.; Sambruna, R.M. A Universal Scaling for the Energetics of Relativistic Jets from Black Hole Systems. *Science* **2012**, *338*, 1445–1448. [\[CrossRef\]](#) [\[PubMed\]](#)

35. Calhau, J.; Sobral, D.; Santos, S.; Matthee, J.; Paulino-Afonso, A.; Stroe, A.; Simmons, B.; Barlow-Hall, C.; Adams, B. The X-ray and radio activity of typical and luminous Ly alpha emitters from $z \sim 2$ to $z \sim 6$: Evidence for a diverse, evolving population. *Mon. Not. R. Astron. Soc.* **2020**, *493*, 3341–3362. [\[CrossRef\]](#)

36. Mizuno, Y.; Gómez, J.L.; Nishikawa, K.-I.; Meli, A.; Hardee, P.E.; Rezzolla, L. Recollimation Shocks in Magnetized Relativistic Jets. *Astrophys. J.* **2015**, *809*, 38. [\[CrossRef\]](#)

37. Sironi, L.; Spitkovsky, A. Relativistic reconnection: An efficient source of non-thermal particles. *Astrophys. J. Lett.* **2014**, *783*, L21. [\[CrossRef\]](#)

38. Porth, O.; Mizuno, Y.; Younsi, Z.; Fromm, C.M. Flares in the Galactic Centre—I. Orbiting flux tubes in magnetically arrested black hole accretion discs. *Mon. Not. R. Astron. Soc.* **2021**, *502*, 2023–2032. [\[CrossRef\]](#)

39. Wardle, J.; Homan, D.C.; Ojha, R.; Roberts, D.H. Electron-positron jets associated with the quasar 3C279. *Nature* **1998**, *395*, 457–461. [\[CrossRef\]](#)

40. Hardcastle, M.J.; Croston, J.H. Radio galaxies and feedback from AGN jets. *New Astron. Rev.* **2020**, *88*, 101539. [\[CrossRef\]](#)

41. Mukherjee, D.; Wagner, A.Y.; Bicknell, G.V.; Morganti, R.; Oosterloo, T.; Nesvadba, N.; Sutherland, R.S. The jet-ISM interactions in IC 5063. *Mon. Not. R. Astron. Soc.* **2018**, *476*, 80–95. [\[CrossRef\]](#)

42. Blackburn, L.; Doebleman, S.; Dexter, J.; Gómez, J.L.; Johnson, M.D.; Palumbo, D.C.; Weintraub, J.; Bouman, K.L.; Chael, A.A.; Farah, J.R.; et al. Studying Black Holes on Horizon Scales with VLBI Ground Arrays. *arXiv* **2019**, arXiv:1909.01411v2. [\[CrossRef\]](#)

43. Johnson, M.D.; Lupsasca, A.; Strominger, A.; Wong, G.N.; Hadar, S.; Kapec, D.; Narayan, R.; Chael, A.; Gammie, C.F.; Galison, P.; et al. Universal interferometric signatures of a black hole's photon ring. *Sci. Adv.* **2020**, *6*, 12. [\[CrossRef\]](#)

44. Palumbo, D.C.M.; Wong, G.N.; Prather, B.S. Discriminating Accretion States via Rotational Symmetry in Simulated Polarimetric Images of M87. *Astrophys. J.* **2020**, *894*, 156. [\[CrossRef\]](#)

45. Roelofs, F.; Janssen, M.; Natarajan, I.; Deane, R.; Davelaar, J.; Olivares, H.; Porth, O.; Paine, S.N.; Bouman, K.L.; Tilanus, R.P.J.; et al. SYMBA: An end-to-end VLBI synthetic data generation pipeline. *Astron. Astrophys.* **2020**, *636*, A5. [\[CrossRef\]](#)

46. The CTA Consortium; Actis, M.; Agnetta, G.; Aharonian, F.; Akhperjanian, A.; Aleksić, J.; Aliu, E.; Allan, D.; Allekotte, I.; Antico, F.; et al. Design concepts for the Cherenkov Telescope Array CTA: An advanced facility for ground-based high-energy gamma-ray astronomy. *Exp. Astron.* **2011**, *32*, 193–316. [\[CrossRef\]](#)

47. CTA Consortium. *Science with the Cherenkov Telescope Array*, 1st ed.; World Scientific: Singapore, 2019; p. 364.

48. Acharya, B.S.; Actis, M.; Aghajani, T.; Agnetta, G.; Aguilar, J.; Aharonian, F.; Ajello, M.; Akhperjanian, A.; Alcubierre, M.; Aleksić, J.; et al. Introducing the CTA concept. *Astropart. Phys.* **2013**, *43*, 3–18. [\[CrossRef\]](#)

49. Abell, P.A.; Allison, J.; Anderson, S.F.; Andrew, J.R.; Angel, J.R.; Armus, L.; Arnett, D.; Asztalos, S.J.; Axelrod, T.S.; Bailey, S.; et al. *LSST Science Book, Version 2.0*, 1st ed.; LSST Science Collaborations and LSST Project: Tucson, AZ, USA, 2009; p. 596.

50. Ivezić, Ž.; Kahn, S.M.; Tyson, J.A.; Abel, B.; Acosta, E.; Allsman, R.; Alonso, D.; AlSayyad, Y.; Anderson, S.F.; Andrew, J.; et al. LSST: From Science Drivers to Reference Design and Anticipated Data Products. *Astrophys. J.* **2019**, *873*, 111. [\[CrossRef\]](#)

51. Brandt, W.N.; Ni, Q.; Yang, G.; Anderson, S.F.; Assef, R.J.; Barth, A.J.; Bauer, F.E.; Bongiorno, A.; Chen, C.T.; De Cicco, D.; et al. Active Galaxy Science in the LSST Deep-Drilling Fields: Footprints, Cadence Requirements, and Total-Depth Requirements. *arXiv* **2018**, arXiv:1811.06542.

52. MacLeod, C.L.; Ivezić, Ž.; Sesar, B.; de Vries, W.; Kochanek, C.S.; Kelly, B.C.; Becker, A.C.; Lupton, R.H.; Hall, P.B.; Richards, G.T.; et al. A description of quasar variability measured using repeated SDSS and POSS Imaging. *Astrophys. J.* **2012**, *753*, 106. [\[CrossRef\]](#)

53. Jorstad, S.G.; Marscher, A.P.; Raiteri, C.M.; Villata, M.; Weaver, Z.R.; Zhang, H.; Dong, L.; Gómez, J.L.; Perel, M.V.; Savchenko, S.S.; et al. Rapid quasi-periodic oscillations in the relativistic jet of BL Lacertae. *Nature* **2022**, *609*, 265–268. [\[CrossRef\]](#)

54. Webb, J.R.; Sanz, I.P. The Structure of Micro-Variability in the WEBT BL Lacertae Observation. *Galaxies* **2023**, *11*, 108. [\[CrossRef\]](#)

55. Blandford, R.; Meier, D.; Readhead, A. Relativistic Jets from Active Galactic Nuclei. *Annu. Rev. Astron. Astrophys.* **2019**, *57*, 467–509. [\[CrossRef\]](#)

56. Chael, A.A.; Johnson, M.D.; Narayan, R.; Doebleman, S.S.; Wardle, J.F.C.; Bouman, K.L. High-Resolution Linear Polarimetric Imaging for the Event Horizon Telescope. *Astrophys. J.* **2016**, *829*, 11. [\[CrossRef\]](#)

57. Ressler, S.M.; Tchekhovskoy, A.; Quataert, E.; Chandra, M.; Gammie, C.F. Electron thermodynamics in GRMHD simulations of low-luminosity black hole accretion. *Mon. Not. R. Astron. Soc.* **2015**, *454*, 1848–1870. [\[CrossRef\]](#)

58. Werner, G.R.; Uzdensky, D.A.; Begelman, M.C.; Cerutti, B.; Nalewajko, K. Non-thermal particle acceleration in collisionless relativistic electron-proton reconnection. *Mon. Not. R. Astron. Soc.* **2017**, *473*, 4840–4861. [\[CrossRef\]](#)

59. Zenitani, S.; Hesse, M.; Klimas, A.; Kuznetsova, M. New Measure of the Dissipation Region in Collisionless Magnetic Reconnection. *Phys. Rev. Lett.* **2011**, *106*, 195003. [\[CrossRef\]](#) [\[PubMed\]](#)

60. Christie, I.M.; Petropoulou, M.; Sironi, L.; Giannios, D. Radiative signatures of plasmoid-dominated reconnection in blazar jets. *Mon. Not. R. Astron. Soc.* **2019**, *482*, 65–82. [\[CrossRef\]](#)

61. Sironi, L.; Spitkovsky, A.; Arons, J. The maximum energy of accelerated particles in relativistic collisionless shocks. *Astrophys. J. Lett.* **2013**, *771*, 54. [\[CrossRef\]](#)

62. Zhdankin, V.; Werner, G.R.; Uzdensky, D.A.; Begelman, M.C. Kinetic Turbulence in Relativistic Plasma: From Thermal Bath to Nonthermal Continuum. *Phys. Rev. Lett.* **2017**, *118*, 055103. [\[CrossRef\]](#)

63. Nakamura, T.K.M.; Genestreti, K.J.; Liu, Y.; Nakamura, R.; Teh, W.; Hasegawa, H.; Daughton, W.; Hesse, M.; Torbert, R.B.; Burch, J.L.; et al. Measurement of the Magnetic Reconnection Rate in the Earth’s Magnetotail. *J. Geophys. Res. Space Phys.* **2018**, *123*, 9150–9168. [\[CrossRef\]](#)

64. Liu, Y.H.; Hesse, M.; Genestreti, K.; Nakamura, R.; Burch, J.L.; Cassak, P.A.; Bessho, N.; Eastwood, J.P.; Phan, T.; Swisdak, M.; et al. Ohm’s law, the reconnection rate, and energy conversion in collisionless magnetic reconnection. *Space Sci. Rev.* **2025**, *221*, 16. [\[CrossRef\]](#)

65. Ripperda, B.; Bacchini, F.; Teunissen, J.; Xia, C.; Porth, O.; Sironi, L.; Lapenta, G.; Keppens, R. A Comprehensive Comparison of Relativistic Particle Integrators. *Astrophys. J. Suppl. Ser.* **2018**, *235*, 21. [\[CrossRef\]](#)

66. Etienne, Z.B.; Liu, Y.T.; Shapiro, S.L. Relativistic magnetohydrodynamics in dynamical spacetimes: A new adaptive mesh refinement implementation. *Mon. Not. R. Astron. Soc.* **2010**, *82*, 084031. [\[CrossRef\]](#)

67. Font, J.A. Numerical hydrodynamics and magnetohydrodynamics in general relativity. *Living Rev. Relativ.* **2008**, *11*, 7. [\[CrossRef\]](#)

68. Liska, M.; Chatterjee, K.; Issa, D.; Yoon, D.; Kaaz, N.; Tchekhovskoy, A.; van Eijnatten, D.; Musoke, G.; Hesp, C.; Rohoza, V.; et al. H-AMR: A New GPU-accelerated GRMHD Code for Exascale Computing with 3D Adaptive Mesh Refinement and Local Adaptive Time Stepping. *Astrophys. J. Suppl. Ser.* **2022**, *263*, 26. [\[CrossRef\]](#)

69. White, C.J.; Stone, J.M.; Gammie, C.F. An Extension of the Athena++ Code Framework for GRMHD Based on Advanced Riemann Solvers and Staggered-Mesh Constrained Transport. *Astrophys. J. Suppl. Ser.* **2016**, *225*, 22. [\[CrossRef\]](#)

70. Doeleman, S.S.; Fish, V.L.; Schenck, D.E.; Beaudoin, C.; Blundell, R.; Bower, G.C.; Broderick, A.E.; Chamberlin, R.; Freund, R.; Friberg, P.; et al. Jet-Launching Structure Resolved Near the Supermassive Black Hole in M87. *Science* **2012**, *338*, 355–358. [\[CrossRef\]](#) [\[PubMed\]](#)

71. Krawczynski, H. Tests of General Relativity in the Strong-gravity Regime Based on X-Ray Spectropolarimetric Observations of Black Holes in X-Ray Binaries. *Astrophys. J.* **2012**, *754*, 133. [\[CrossRef\]](#)

72. Psaltis, D.; Medeiros, L.; Christian, P.; Özel, F.; Akiyama, K.; Alberdi, A.; Alef, W.; Asada, K.; Azulay, R.; Ball, D.; et al. Gravitational Test beyond the First Post-Newtonian Order with the Shadow of the M87 Black Hole. *Phys. Rev. Lett.* **2020**, *125*, 141104. [\[CrossRef\]](#)

73. The Event Horizon Telescope Collaboration; Akiyama, K.; Alberdi, A.; Alef, W.; Asada, K.; Azulay, R.; Baczko, A.K.; Ball, D.; Baloković, M.; Barrett, J.; et al. First M87 Event Horizon Telescope Results. II. Array and Instrumentation. *Astrophys. J. Lett.* **2019**, *875*, L2.

74. Narayan, R.; Palumbo, D.C.M.; Johnson, M.D.; Gelles, Z.; Himwich, E.; Chang, D.O.; Ricarte, A.; Dexter, J.; Gammie, C.F.; Chael, A.A.; et al. The Polarized Image of a Synchrotron-emitting Ring of Gas Orbiting a Black Hole. *Astrophys. J.* **2021**, *912*, 35. [\[CrossRef\]](#)

75. Christie, I.M. The role of magnetic field geometry in the evolution of neutron star merger accretion discs. *Mon. Not. R. Astron. Soc.* **2019**, *490*, 4811–4825. [\[CrossRef\]](#)

76. Raymond, A.W.; Palumbo, D.; Paine, S.N.; Blackburn, L.; Rosado, R.C.; Doeleman, S.S.; Farah, J.R.; Johnson, M.D.; Roelofs, F.; Tilanus, R.P.J.; et al. Evaluation of new submillimeter VLBI sites for the Event Horizon Telescope. *Astrophys. J. Suppl. Ser.* **2021**, *253*, 5. [\[CrossRef\]](#)

77. Issaoun, S.; Johnson, M.D.; Blackburn, L.; Brinkerink, C.D.; Mościbrodzka, M.; Chael, A.; Goddi, C.; Martí-Vidal, I.; Wagner, J.; Doeleman, S.S.; et al. The Size, Shape, and Scattering of Sagittarius A* at 86 GHz: First VLBI with ALMA. *Astrophys. J.* **2019**, *871*, 30. [\[CrossRef\]](#)

78. Bower, G.C.; Wright, M.C.H.; Falcke, H.; Backer, D.C. Interferometric detection of linear polarization from Sagittarius A* at 230 GHz. *Astrophys. J.* **2003**, *588*, 331. [\[CrossRef\]](#)

79. Ortiz-León, G.N.; Johnson, M.D.; Doeleman, S.S.; Blackburn, L.; Fish, V.L.; Loinard, L.; Reid, M.J.; Castillo, E.; Chael, A.A.; Hernández-Gómez, A.; et al. The intrinsic shape of Sagittarius A* at 3.5 mm wavelength. *Astron. Astrophys.* **2016**, *824*, 40. [\[CrossRef\]](#)

80. Do, T.; Hees, A.; Ghez, A.; Martinez, G.D.; Chu, D.S.; Jia, S.; Sakai, S.; Lu, J.R.; Gautam, A.K.; O’Neil, K.K.; et al. Relativistic redshift of the star S0-2 orbiting the Galactic Center supermassive black hole. *Science* **2019**, *365*, 664–668. [\[CrossRef\]](#)

81. Wielgus, M.; Akiyama, K.; Blackburn, L.; Chan, C.-K.; Dexter, J.; Doeleman, S.S.; Fish, V.L.; Issaoun, S.; Johnson, M.D.; Krichbaum, T.P.; et al. Monitoring the Morphology of M87* in 2009–2017 with the Event Horizon Telescope. *Astrophys. J.* **2020**, *901*, 67. [\[CrossRef\]](#)

82. Doeleman, S.; Weintraub, J.; Rogers, A.E.E.; Plambeck, R.; Freund, R.; Tilanus, R.P.J.; Friberg, P.; Ziurys, L.M.; Moran, J.M.; Corey, B.; et al. Event-horizon-scale structure in the supermassive black hole candidate at the Galactic Centre. *Nature* **2008**, *455*, 78–80. [\[CrossRef\]](#)

83. Gold, R.; McKinney, J.C.; Johnson, M.D.; Doeleman, S.S. Probing the magnetic field structure in Sgr A* on black hole horizon scales with polarized radiative transfer simulations. *Astrophys. J.* **2017**, *837*, 180. [\[CrossRef\]](#)

84. Bower, G.C.; Falcke, H.; Herrnstein, R.M.; Zhao, J.-H.; Goss, W.M.; Backer, D.C. Detection of the Intrinsic Size of Sagittarius A* Through Closure Amplitude Imaging. *Science* **2004**, *304*, 704–708. [\[CrossRef\]](#)

85. Marrone, D.P.; Moran, J.M.; Zhao, J.-H.; Rao, R. An Unambiguous Detection of Faraday Rotation in Sagittarius A*. *Astrophys. J.* **2007**, *654*, L57. [\[CrossRef\]](#)

86. Mościbrodzka, M.; Falcke, H.; Shiokawa, H.; Gammie, C.F. Observational appearance of inefficient accretion flows and jets in 3D GRMHD simulations: Application to Sagittarius A*. *Astron. Astrophys.* **2014**, *570*, A7. [\[CrossRef\]](#)

87. Muñoz, D.J.; Marrone, D.P.; Moran, J.M.; Rao, R. The Circular Polarization of Sagittarius A* at Submillimeter Wavelengths. *Astrophys. J.* **2012**, *745*, 115. [\[CrossRef\]](#)

88. Goddi, C.; Falcke, H.; Kramer, M.; Rezzolla, L.; Brinkerink, C.; Bronzwaer, T.; Davelaar, J.R.J.; Deane, R.; De Laurentis, M.; Desvignes, G.; et al. BlackHoleCam: Fundamental physics of the galactic center. *Int. J. Mod. Phys. D* **2017**, *26*, 1730001. [\[CrossRef\]](#)

89. Plambeck, R.L.; Bower, G.C.; Rao, R.; Marrone, D.P.; Jorstad, S.G.; Marscher, A.P.; Doeleman, S.S.; Fish, V.L.; Johnson, M.D. Probing the Parsec-Scale Accretion Flow of 3C 84 with Millimeter Wavelength Polarimetry. *Astrophys. J.* **2014**, *797*, 66. [\[CrossRef\]](#)

90. Chael, A.A.; Johnson, M.D.; Bouman, K.L.; Blackburn, L.L.; Akiyama, K.; Narayan, R. Interferometric Imaging Directly with Closure Phases and Closure Amplitudes. *Astrophys. J.* **2018**, *857*, 23. [\[CrossRef\]](#)

91. Mościbrodzka, M.; Dexter, J.; Davelaar, J.; Falcke, H. Faraday rotation in GRMHD simulations of the jet launching zone of M87. *Mon. Not. R. Astron. Soc.* **2017**, *468*, 2214–2221. [\[CrossRef\]](#)

92. Finke, J.D.; Razzaque, S.; Dermer, C.D. Modeling the extragalactic background light from stars and dust. *Astrophys. J.* **2010**, *712*, 238. [\[CrossRef\]](#)

93. Lidman, C.; Rosati, P.; Demarco, R.; Nonino, M.; Mainieri, V.; Stanford, S.A.; Toft, S. Deep near-infrared imaging of RDCS J1252. 9–2927 at $z = 1.237^*$ —The colour-magnitude diagram. *Astron. Astrophys.* **2004**, *416*, 829–837. [\[CrossRef\]](#)

94. Aharonian, F.; Akhperjanian, A.G.; Anton, G.; de Almeida, U.B.; Bazer-Bachi, A.R.; Becherini, Y.; Behera, B.; Bernlöhr, K.; Boisson, C.; Bochow, A.; et al. Simultaneous observations of PKS 2155-304 with H.E.S.S., Fermi, RXTE, and ATOM: Spectral energy distributions and variability in a low state. *Astrophys. J. Lett.* **2009**, *696*, L150. [\[CrossRef\]](#)

95. Albert, J.; Aliu, E.; Anderhub, H.; Antonelli, L.A.; Antoranz, P.; Backes, M.; Baixeras, C.; Barrio, J.A.; Bartko, H.; Bastieri, D.; et al. Very high energy gamma-ray observations of strong flaring activity in M87 in 2008 February. *Astrophys. J. Lett.* **2008**, *685*, L23. [\[CrossRef\]](#)

96. Giannios, D.; Uzdensky, D.A.; Begelman, M.C. Fast TeV variability in blazars: Jets in a jet. *Mon. Not. R. Astron. Soc. Lett.* **2009**, *395*, L29–L33. [\[CrossRef\]](#)

97. Sharma, A.; Prince, R.; Bose, D. From microquasars to AGN: A uniform jet variability. *Phys. Rev. D* **2025**, *111*, 083049. [\[CrossRef\]](#)

98. Nalewajko, K.; Giannios, D.; Begelman, M.C.; Uzdensky, D.A.; Sikora, M. Radiative properties of reconnection-powered minijets in blazars. *Mon. Not. R. Astron. Soc.* **2011**, *413*, 333–346. [\[CrossRef\]](#)

99. Abramowski, A.; Stinzing, F.; Huan, H.; Aune, T.; Feinstein, F.; Vorster, M.; Maneva, G.; Hui, C.M.; Hofverberg, P.; Perlman, E.S.; et al. The 2010 very high energy γ -ray flare and 10 years of multi-wavelength observations of M 87. *Astrophys. J.* **2012**, *746*, 151. [\[CrossRef\]](#)

100. MAGIC Collaboration; Aleksić, J.; Antonelli, L.A.; Antoranz, P.; Backes, M.; Barrio, J.A.; Bastieri, D.; González, J.B.; Bednarek, W.; Berdyugin, A.; et al. Detection of very high energy γ -ray emission from the Perseus cluster head-tail galaxy IC 310 by the MAGIC telescopes. *Astrophys. J. Lett.* **2012**, *723*, L207. [\[CrossRef\]](#)

101. Veritas Collaboration; VLBA 43 GHz M87 Monitoring Team; HESS Collaboration; Magic Collaboration; Acciari, V.A.; Aliu, E.; Arlen, T.; Bautista, M.; Beilicke, M.; Benbow, W.; et al. Radio imaging of the very-high-energy γ -ray emission region in the central engine of a radio galaxy. *Science* **2009**, *325*, 444–448.

102. Aharonian, F.; Akhperjanian, A.G.; Bazer-Bachi, A.R.; Beilicke, M.; Benbow, W.; Berge, D.; Bernlöhr, K.; Boisson, C.; Bolz, O.; Borrel, V.; et al. Fast variability of tera-electron volt γ rays from the radio galaxy M87. *Science* **2006**, *314*, 1424–1427. [\[CrossRef\]](#)

103. Hardcastle, M.J.; Evans, D.A.; Croston, J.H. The active nuclei of $z < 1.0$ 3CRR radio sources. *Mon. Not. R. Astron. Soc.* **2009**, *396*, 1929–1952.

104. Stawarz, Ł.; Aharonian, F.; Kataoka, J.; Ostrowski, M.; Siemiginowska, A.; Sikora, M. Dynamics and high-energy emission of the flaring HST-1 knot in the M 87 jet. *Mon. Not. R. Astron. Soc.* **2006**, *370*, 981–992. [\[CrossRef\]](#)

105. Aartsen, M.G.; Ackermann, M.; Adams, J.; Aguilar, J.; Ahlers, M.; Ahrens, M.; Altmann, D.; Andeen, K.; Anderson, T.; Ansseau, I.; et al. The IceCube Neutrino Observatory: Instrumentation and online systems. *J. Instrum.* **2017**, *12*, P03012. [\[CrossRef\]](#)

106. IceCube Collaboration. Neutrino emission from the direction of the blazar TXS 0506+056 prior to the IceCube-170922A alert. *Science* **2018**, *361*, 147–151. [\[CrossRef\]](#) [\[PubMed\]](#)

107. Petropoulou, M.; Psarras, F.; Giannios, D. Hadronic signatures from magnetically dominated baryon-loaded AGN jets. *Mon. Not. R. Astron. Soc.* **2023**, *518*, 2719–2734. [\[CrossRef\]](#)

108. Petropoulou, M.; Dimitrakoudis, S.; Padovani, P.; Mastichiadis, A.; Resconi, E. Photohadronic origin of γ -ray BL Lac emission: Implications for IceCube neutrinos. *Mon. Not. R. Astron. Soc.* **2015**, *448*, 2412–2429. [\[CrossRef\]](#)

109. Padovani, P.; Giommi, P.; Resconi, E.; Glauch, T.; Arsioli, B.; Sahakyan, N.; Huber, M. Dissecting the region around IceCube-170922A: The blazar TXS 0506+056 as the first cosmic neutrino source. *Mon. Not. R. Astron. Soc.* **2018**, *480*, 192–203. [\[CrossRef\]](#)

110. Rodrigues, X.; Fedynitch, A.; Gao, S.; Boncioli, D.; Winter, W. Neutrinos and Ultra-high-energy Cosmic-ray Nuclei from Blazars. *Astrophys. J.* **2018**, *854*, 54. [\[CrossRef\]](#)

111. Kathirgamaraju, A.; Duran, R.B.; Giannios, D. Off-axis short GRBs from structured jets as counterparts to GW events. *Mon. Not. R. Astron. Soc. Lett.* **2017**, *473*, L121–L125. [\[CrossRef\]](#)

112. Metzger, B.D.; Martínez-Pinedo, G.; Darbha, S.; Quataert, E.; Arcones, A.; Kasen, D.; Thomas, R.; Nugent, P.; Panov, I.V.; Zinner, N.T. Electromagnetic counterparts of compact object mergers powered by the radioactive decay of r-process nuclei. *Mon. Not. R. Astron. Soc.* **2010**, *406*, 2650–2662. [\[CrossRef\]](#)

113. Bartos, I.; Kowalski, M. *Multimessenger Astronomy*; IOP Publishing Ltd.: Bristol, UK, 2017; p. 26.

114. Jorstad, S.G.; Marscher, A.P.; Larionov, V.M.; Agudo, I.; Smith, P.S.; Gurwell, M.; Lähteenmäki, A.; Tornikoski, M.; Markowitz, A.; Arkharov, A.A.; et al. Flaring behavior of the quasar 3C 454.3 across the electromagnetic spectrum. *Astrophys. J.* **2010**, *715*, 362. [\[CrossRef\]](#)

115. Ota, N.; Murase, K.; Kitayama, T.; Komatsu, E.; Hattori, M.; Matsuo, H.; Oshima, T.; Suto, Y.; Yoshikawa, K. Suzaku broad-band spectroscopy of RX J1347.5-1145: Constraints on the extremely hot gas and non-thermal emission. *Astron. Astrophys.* **2008**, *491*, 363–377. [\[CrossRef\]](#)

116. Tavecchio, F.; Maraschi, L.; Pian, E.; Chiappetti, L.; Celotti, A.; Fossati, G.; Ghisellini, G.; Palazzi, E.; Raiteri, C.M.; Sambruna, R.M.; et al. Theoretical Implications from the Spectral Evolution of Markarian 501 Observed with BeppoSAX. *Astrophys. J.* **2001**, *554*, 725. [\[CrossRef\]](#)

117. Sikora, M.; Stawarz, Ł.; Moderski, R.; Nalewajko, K.; Madejski, G.M. Constraining emission models of luminous blazar sources. *Astrophys. J.* **2009**, *704*, 38. [\[CrossRef\]](#)

118. Kaiser, C.R. Cherenkov Telescope Array Status Report. *arXiv* **2017**, arXiv:1705.07805

119. CTA (Cherenkov Telescope Array). Available online: <https://www.eoportal.org/other-space-activities/cta> (accessed on 29 December 2025).

120. Schwamb, M.E.; Jones, R.L.; Yoachim, P.; Volk, K.; Dorsey, R.C.; Opitom, C.; Greenstreet, S.; Lister, T.; Snodgrass, C.; Bolin, B.T.; et al. Tuning the Legacy Survey of Space and Time (LSST) Observing Strategy for Solar System Science. *Astrophys. J. Suppl. Ser.* **2023**, *266*, 22. [\[CrossRef\]](#)

121. Caplar, N.; Lilly, S.J.; Trakhtenbrot, B. Optical Variability of AGNs in the PTF/iPTF Survey. *Astrophys. J.* **2017**, *834*, 111. [\[CrossRef\]](#)

122. Hickox, R.C.; Mullaney, J.R.; Alexander, D.M.; Chen, C.-T.J.; Civano, F.M.; Goulding, A.D.; Hainline, K.N. Black hole variability and the star formation-active galactic nucleus connection: Do all star-forming galaxies host an active galactic nucleus? *Astrophys. J.* **2014**, *782*, 9. [\[CrossRef\]](#)

123. Schawinski, K.; Urry, C.M.; Simmons, B.D.; Fortson, L.; Kaviraj, S.; Keel, W.C.; Lintott, C.J.; Masters, K.L.; Nichol, R.C.; Sarzi, M.; et al. The green valley is a red herring: Galaxy Zoo reveals two evolutionary pathways towards quenching of star formation in early- and late-type galaxies. *Mon. Not. R. Astron. Soc.* **2014**, *440*, 889–907. [\[CrossRef\]](#)

124. Best, P.N.; Heckman, T.M. On the fundamental dichotomy in the local radio-AGN population: Accretion, evolution and host galaxy properties. *Mon. Not. R. Astron. Soc.* **2012**, *421*, 1569–1582. [\[CrossRef\]](#)

125. Sabater, J.; Best, P.N.; Hardcastle, M.J.; Shimwell, T.W.; Tasse, C.; Williams, W.L.; Brüggen, M.; Cochrane, R.K.; Croston, J.H.; de Gasperin, F.; et al. The LoTSS view of radio AGN in the local Universe. The most massive galaxies are always switched on. *Astron. Astrophys.* **2019**, *622*, A17. [\[CrossRef\]](#)

126. Martini, P.; Sivakoff, G.R.; Mulchaey, J.S. The evolution of active galactic nuclei in clusters of galaxies to redshift 1.3. *Astrophys. J.* **2009**, *701*, 66. [\[CrossRef\]](#)

127. Schulze, A.; Bongiorno, A.; Gavignaud, I.; Schramm, M.; Silverman, J.; Merloni, A.; Zamorani, G.; Hirschmann, M.; Mainieri, V.; Wisotzki, L.; et al. The cosmic growth of the active black hole population at $1 < z < 2$ in zCOSMOS, VVDS and SDSS. *Mon. Not. R. Astron. Soc.* **2015**, *447*, 2085–2111. [\[CrossRef\]](#)

128. Mosta, P.; Radice, D.; Haas, R.; Schnetter, E.; Bernuzzi, S. A magnetar engine for short GRBs and kilonovae. *Astrophys. J. Lett.* **2020**, *901*, L37. [\[CrossRef\]](#)

129. Komossa, S. Tidal disruption of stars by supermassive black holes: Status of observations. *J. High Energy Astrophys.* **2015**, *7*, 148–157. [\[CrossRef\]](#)

130. Nugent, A.E.; Fong, W.-F.; Castrejon, C.; Leja, J.; Zevin, M.; Ji, A.P. A Population of Short-duration Gamma-Ray Bursts with Dwarf Host Galaxies. *Astrophys. J.* **2024**, *962*, 5. [\[CrossRef\]](#)

131. Tchekhovskoy, A.; Bromberg, O. Three-dimensional relativistic MHD simulations of active galactic nuclei jets: Magnetic kink instability and Fanaroff–Riley dichotomy. *Mon. Not. R. Astron. Soc. Lett.* **2016**, *461*, L46–L50. [\[CrossRef\]](#)

132. Auchettl, K.; Guillochon, J.; Ramirez-Ruiz, E. New Physical Insights about Tidal Disruption Events from a Comprehensive Observational Inventory at X-Ray Wavelengths. *Astrophys. J.* **2017**, *838*, 149. [\[CrossRef\]](#)

133. Van Velzen, S.; Farrar, G.R.; Gezari, S.; Morrell, N.; Zaritsky, D.; Östman, L.; Smith, M.; Gelf, J.; Drake, A.J. Optical discovery of probable stellar tidal disruption flares. *Astrophys. J.* **2011**, *741*, 73. [\[CrossRef\]](#)

134. Harrison, C.M.; Costa, T.; Tadhunter, C.N.; Flütsch, A.; Kakkad, D.; Perna, M.; Vietri, G. AGN outflows and feedback twenty years on. *Nat. Astron.* **2018**, *2*, 198–205. [\[CrossRef\]](#)

135. Ellison, S.L.; Jones, C.; Forman, W.R.; Murray, S.S.; Kochanek, C.S.; Eisenstein, D.; Jannuzzi, B.T.; Dey, A.; Brown, M.J.I.; Stern, D.; et al. Galaxy pairs in the Sloan Digital Sky Survey—IV. Interactions trigger active galactic nuclei. *Mon. Not. R. Astron. Soc.* **2011**, *418*, 2043–2053. [\[CrossRef\]](#)

136. Hickox, R.C.; Jones, C.; Forman, W.R.; Murray, S.S.; Kochanek, C.S.; Eisenstein, D.; Jannuzzi, B.T.; Dey, A.; Brown, M.J.I.; Stern, D.; et al. Host galaxies, clustering, Eddington ratios, and evolution of radio, X-ray, and infrared-selected AGNs. *Astrophys. J.* **2009**, *696*, 891. [\[CrossRef\]](#)

137. Bower, G.C.; Schaye, J.; Frenk, C.S.; Theuns, T.; Schaller, M.; Crain, R.A.; McAlpine, S. The dark nemesis of galaxy formation: Why hot haloes trigger black hole growth and bring star formation to an end. *Mon. Not. R. Astron. Soc.* **2017**, *465*, 32–44. [\[CrossRef\]](#)

138. Croton, D.J.; Springel, V.; White, S.D.M.; De Lucia, G.; Frenk, C.S.; Gao, L.; Jenkins, A.; Kauffmann, G.; Navarro, J.F.; Yoshida, N. The many lives of active galactic nuclei: Cooling flows, black holes and the luminosities and colours of galaxies. *Mon. Not. R. Astron. Soc.* **2006**, *365*, 11–28. [\[CrossRef\]](#)

139. Graham, M.J.; Ross, N.P.; Stern, D.; Drake, A.J.; McKernan, B.; Ford, K.E.S.; Djorgovski, S.G.; A Mahabal, A.; Glikman, E.; Larson, S.; et al. Understanding extreme quasar optical variability with CRTS—II. Changing-state quasars. *Mon. Not. R. Astron. Soc.* **2020**, *491*, 4925–4948. [\[CrossRef\]](#)

140. Bañados, E.; Venemans, B.P.; Mazzucchelli, C.; Farina, E.P.; Walter, F.; Wang, F.; Decarli, R.; Stern, D.; Fan, X.; Davies, F.B.; et al. An 800-million-solar-mass black hole in a significantly neutral Universe at a redshift of 7.5. *Nature* **2018**, *553*, 473–476. [\[CrossRef\]](#) [\[PubMed\]](#)

141. Volonteri, M.; Haardt, F.; Madau, P. The Assembly and Merging History of Supermassive Black Holes in Hierarchical Models of Galaxy Formation. *Astrophys. J.* **2003**, *582*, 559. [\[CrossRef\]](#)

142. Di Matteo, T.; Springel, V.; Hernquist, L. Energy input from quasars regulates the growth and activity of black holes and their host galaxies. *Nature* **2005**, *433*, 604–607. [\[CrossRef\]](#)

143. Hopkins, P.F.; Hernquist, L.; Cox, T.J.; Di Matteo, T.; Robertson, B.; Springel, V. A Unified, Merger-driven Model of the Origin of Starbursts, Quasars, the Cosmic X-Ray Background, Supermassive Black Holes, and Galaxy Spheroids. *Astrophys. J. Suppl. Ser.* **2006**, *163*, 1. [\[CrossRef\]](#)

144. Bentz, M.C.; Denney, K.D.; Grier, C.J.; Barth, A.J.; Peterson, B.M.; Vestergaard, M.; Bennert, V.N.; Canalizo, G.; De Rosa, G.; Filippenko, A.V.; et al. The low-luminosity end of the radius–luminosity relationship for active galactic nuclei. *Astrophys. J.* **2013**, *767*, 149. [\[CrossRef\]](#)

145. Peterson, B.M.; Ferrarese, L.; Gilbert, K.M.; Kaspi, S.; Malkan, M.A.; Maoz, D.; Merritt, D.; Netzer, H.; Onken, C.A.; Pogge, R.W.; et al. Central Masses and Broad-Line Region Sizes of Active Galactic Nuclei. II. A Homogeneous Analysis of a Large Reverberation-Mapping Database. *Astrophys. J.* **2004**, *613*, 682. [\[CrossRef\]](#)

146. Fausnaugh, M.M.; Denney, K.D.; Barth, A.J.; Bentz, M.C.; Bottorff, M.C.; Carini, M.T.; Croxall, K.V.; De Rosa, G.; Goad, M.R.; Horne, K.; et al. Space Telescope and Optical Reverberation Mapping Project. III. Optical continuum emission and broad-band time delays in NGC 5548. *Astrophys. J.* **2016**, *821*, 56. [\[CrossRef\]](#)

147. Grier, C.J.; Peterson, B.M.; Horne, K.; Bentz, M.C.; Pogge, R.W.; Denney, K.D.; De Rosa, G.; Martini, P.; Kochanek, C.S.; Zu, Y.; et al. The structure of the broad-line region in active galactic nuclei. I. Reconstructed velocity-delay maps. *Astrophys. J.* **2013**, *764*, 47. [\[CrossRef\]](#)

148. Mészáros, P.; Fox, D.B.; Hanna, C.; Murase, K. Multi-messenger astrophysics. *Nat. Rev. Phys.* **2019**, *1*, 585–599. [\[CrossRef\]](#)

149. Fuhrmann, L.; Larsson, S.; Chiang, J.; Angelakis, E.; Zensus, J.A.; Nestoras, I.; Krichbaum, T.P.; Ungerechts, H.; Sievers, A.; Pavlidou, V.; et al. Detection of significant cm to sub-mm band radio and gamma-ray correlated variability in Fermi bright blazars. *Mon. Not. R. Astron. Soc.* **2014**, *441*, 1899–1909. [\[CrossRef\]](#)

150. Max-Moerbeck, W.; Hovatta, T.; Richards, J.L.; King, O.G.; Pearson, T.J.; Readhead, A.C.S.; Reeves, R.; Shepherd, M.C.; Stevenson, M.A.; Angelakis, E.; et al. Time correlation between the radio and gamma-ray activity in blazars and the production site of the gamma-ray emission. *Mon. Not. R. Astron. Soc.* **2014**, *445*, 428–436. [\[CrossRef\]](#)

151. Bellm, E.C.; Kulkarni, S.R.; Graham, M.J.; Dekany, R.; Smith, R.M.; Riddle, R.; Masci, F.J.; Helou, G.; Prince, T.A.; Adams, S.M.; et al. The Zwicky Transient Facility: System Overview, Performance, and First Results. *Publ. Astron. Soc. Pac.* **2018**, *131*, 018002. [\[CrossRef\]](#)

152. Perna, R.; Lazzati, D.; Giacomazzo, B. Short gamma-ray bursts from the merger of two black holes. *Astrophys. J. Lett.* **2016**, *821*, L18. [\[CrossRef\]](#)

153. Ciolfi, R.; Kastaun, W.; Giacomazzo, B.; Endrizzi, A.; Siegel, D.M.; Perna, R. General relativistic magnetohydrodynamic simulations of binary neutron star mergers forming a long-lived neutron star. *Phys. Rev. D* **2017**, *95*, 063016. [\[CrossRef\]](#)

154. Ruiz, M.; Lang, R.N.; Paschalidis, V.; Shapiro, S.L. Binary neutron star mergers: A jet engine for short gamma-ray bursts. *Astrophys. J. Lett.* **2016**, *824*, L6. [\[CrossRef\]](#)

155. Amaro-Seoane, P.; Audley, H.; Babak, S.; Baker, J.; Barausse, E.; Bender, P.; Berti, E.; Binetruy, P.; Born, M.; Bortoluzzi, D.; et al. Laser Interferometer Space Antenna. *arXiv* **2017**, arXiv:1702.00786. [\[CrossRef\]](#)

156. Haiman, Z. Electromagnetic chirp of a compact binary black hole: A phase template for the gravitational wave inspiral. *Phys. Rev. D* **2017**, *96*, 023004. [\[CrossRef\]](#)

157. Palenzuela, C.; Lehner, L.; Ponce, M.; Liebling, S.L.; Anderson, M.; Nielsen, D.; Motl, P. Electromagnetic and Gravitational Outputs from Binary-Neutron-Star Coalescence. *Phys. Rev. Lett.* **2013**, *111*, 061105. [\[CrossRef\]](#)

158. Baron, D. Machine Learning in Astronomy: A practical overview. *arXiv* **2019**, arXiv:1904.07248v1. [\[CrossRef\]](#)

159. Bloom, J.S.; Richards, J.W.; Nugent, P.E.; Quimby, R.M.; Kasliwal, M.M.; Starr, D.L.; Poznanski, D.; Ofek, E.O.; Cenko, S.B.; Butler, N.R.; et al. Automating Discovery and Classification of Transients and Variable Stars in the Synoptic Survey Era. *Publ. Astron. Soc. Pac.* **2012**, *124*, 1175. [\[CrossRef\]](#)

160. Belloni, T.; Homan, J.; Casella, P.; van der Klis, M.; Nespoli, E.; Lewin, W.H.G.; Miller, J.M.; Méndez, M. The evolution of the timing properties of the black-hole transient GX 339–4 during its 2002/2003 outburst. *Astron. Astrophys.* **2005**, *440*, 207–222. [\[CrossRef\]](#)

161. Fender, R.P.; Homan, J.; Belloni, T.M. Jets from black hole X-ray binaries: Testing, refining and extending empirical models for the coupling to X-rays. *Mon. Not. R. Astron. Soc.* **2009**, *396*, 1370–1382. [\[CrossRef\]](#)

162. Fender, R.; Belloni, T. Stellar-Mass Black Holes and Ultraluminous X-ray Sources. *Science* **2012**, *337*, 540–544. [\[CrossRef\]](#)

163. Remillard, R.A.; McClintock, J.E. X-Ray Properties of Black-Hole Binaries. *Annu. Rev. Astron. Astrophys.* **2006**, *44*, 49–92. [\[CrossRef\]](#)

164. Gallo, E.; Fender, R.; Kaiser, C.; Russell, D.; Morganti, R.; Oosterloo, T.; Heinz, S. A dark jet dominates the power output of the stellar black hole Cygnus X-1. *Nature* **2005**, *436*, 819–821. [\[CrossRef\]](#)

165. Mirabel, I.; Rodríguez, L. A superluminal source in the Galaxy. *Nature* **1994**, *371*, 46–48. [\[CrossRef\]](#)

166. Fender, R.P.; Belloni, T.M.; Gallo, E. Towards a unified model for black hole X-ray binary jets. *Mon. Not. R. Astron. Soc.* **2004**, *355*, 1105–1118. [\[CrossRef\]](#)

167. Ho, L.C.; Wang, J.W. *The Central Engine of Active Galactic Nuclei*, 1st ed.; Conference Series; Astronomical Society of the Pacific: San Francisco, CA, USA, 2007; Volume 373.

168. Merloni, A.; Keppens, R. Decelerating relativistic two-component jets. *Mon. Not. R. Astron. Soc.* **2003**, *345*, 1057–1076. [\[CrossRef\]](#)

169. Gultekin, K.; King, A.L.; Cackett, E.M.; Nyland, K.; Miller, J.M.; Di Matteo, T.; Markoff, S.; Rupen, M.P. The Fundamental Plane of Black Hole Accretion and Its Use as a Black Hole-Mass Estimator. *Astrophys. J.* **2019**, *871*, 80. [\[CrossRef\]](#)

170. Plotkin, R.M.; Gallo, E.; Jonker, P.G. The X-Ray Spectral Evolution of Galactic Black Hole X-Ray Binaries toward Quiescence. *Astrophys. J.* **2013**, *773*, 59. [\[CrossRef\]](#)

171. Kumar, P.; Zhang, B. The physics of gamma-ray bursts & relativistic jets. *Phys. Rep.* **2015**, *561*, 1–109. [\[CrossRef\]](#)

172. Piran, T. The physics of gamma-ray bursts. *Rev. Mod. Phys.* **2005**, *76*, 1143. [\[CrossRef\]](#)

173. Berger, E. Short-duration gamma-ray bursts. *Annu. Rev. Astron. Astrophys.* **2014**, *52*, 43–105. [\[CrossRef\]](#)

174. Woosley, S.E.; Bloom, J.S. Monitoring the Morphology of M87* in 2009–2017 with the Event Horizon Telescope. The Supernova–Gamma-Ray Burst Connection. *Annu. Rev. Astron. Astrophys.* **2006**, *44*, 507–556. [\[CrossRef\]](#)

175. Abbott, B.P.; Abbott, R.; Abbott, T.D.; Acernese, F.; Ackley, K.; Adams, C.; Adams, T.; Addesso, P.; Adhikari, R.X.; Adya, V.B.; et al. GW170817: Observation of gravitational waves from a binary neutron star inspiral. *Phys. Rev. Lett.* **2017**, *119*, 161101. [\[CrossRef\]](#)

176. Goldstein, A.; Veres, P.; Burns, E.; Briggs, M.S.; Hamburg, R.; Kocevski, D.; Wilson-Hodge, C.A.; Preece, R.D.; Poolakkil, S.; Roberts, O.J.; et al. An ordinary short gamma-ray burst with extraordinary implications: Fermi-GBM detection of GRB 170817A. *Astrophys. J. Lett.* **2017**, *848*, L14. [\[CrossRef\]](#)

177. Lazzati, D.; Perna, R.; Morsanyi, B.J.; Lopez-Camara, D.; Cantiello, M.; Ciolfi, R.; Giacomazzo, B.; Workman, J.C. Late Time Afterglow Observations Reveal a Collimated Relativistic Jet in the Ejecta of the Binary Neutron Star Merger GW170817. *Phys. Rev. Lett.* **2018**, *120*, 241103. [\[CrossRef\]](#)

178. Mooley, K.P.; Deller, A.T.; Gottlieb, O.; Nakar, E.; Hallinan, G.; Bourke, S.; Frail, D.A.; Horesh, A.; Corsi, A.; Hotokezaka, K. Superluminal motion of a relativistic jet in the neutron-star merger GW170817. *Nature* **2018**, *561*, 355–359. [\[CrossRef\]](#)

179. Cucchiara, A.; Levan, A.J.; Fox, D.B.; Tanvir, N.R.; Ukwatta, T.N.; Berger, E.; Krühler, T.; Yoldaş, A.K.; Wu, X.F.; Toma, K.; et al. A Photometric Redshift of $z \sim 9.4$ for GRB 090429B. *Astrophys. J.* **2006**, *736*, 7. [\[CrossRef\]](#)

180. Tanvir, N.R.; Fox, D.B.; Levan, A.J.; Berger, E.; Wiersema, K.; Fynbo, J.P.; Cucchiara, A.; Krühler, T.; Gehrels, N.; Bloom, J.S.; et al. A γ -ray burst at a redshift of $z \approx 8.2$. *Nature* **2009**, *461*, 1254–1257. [\[CrossRef\]](#)

181. Perley, D.A.; Krühler, T.; Schulze, S.; Postigo, A.d.U.; Hjorth, J.; Berger, E.; Cenko, S.B.; Chary, R.; Cucchiara, A.; Ellis, R.; et al. The Swift GRB host galaxy legacy survey. I. Sample selection and redshift distribution. *Astrophys. J.* **2016**, *817*, 7. [\[CrossRef\]](#)

182. Salvaterra, R.; Campana, S.; Vergani, S.D.; Covino, S.; D’Avanzo, P.; Fugazza, D.; Ghirlanda, G.; Ghisellini, G.; Melandri, A.; Nava, L.; et al. A complete sample of bright swift long gamma-ray bursts. I. Sample presentation, luminosity function and evolution. *Astrophys. J.* **2012**, *749*, 68. [\[CrossRef\]](#)

183. Phinney, E.S. Manifestations of a Massive Black Hole in the Galactic Center. *Symp.-Int. Astron. Union* **1989**, *136*, 543–553. [\[CrossRef\]](#)

184. Rees, M. Tidal disruption of stars by black holes of 10^6 – 10^8 solar masses in nearby galaxies. *Nature* **1988**, *333*, 523–528. [\[CrossRef\]](#)

185. Bloom, J.S.; Giannios, D.; Metzger, B.D.; Cenko, S.B.; Perley, D.A.; Butler, N.R.; Tanvir, N.R.; Levan, A.J.; Brien, P.T.O.; Strubbe, L.E.; et al. A Possible Relativistic Jetted Outburst from a Massive Black Hole Fed by a Tidally Disrupted Star. *Annu. Rev. Astron. Astrophys.* **2011**, *333*, 203–206. [\[CrossRef\]](#)

186. Burrows, D.N.; Kennea, J.A.; Ghisellini, G.; Mangano, V.; Zhang, B.; Page, K.L.; Eracleous, M.; Romano, P.; Sakamoto, T.; Falcone, A.D.; et al. Relativistic jet activity from the tidal disruption of a star by a massive black hole. *Nature* **2011**, *476*, 421–424. [\[CrossRef\]](#)

187. Jorstad, S.G.; Marscher, A.P.; Morozova, D.A.; Troitsky, I.S.; Agudo, I.; Casadio, C.; Foord, A.; Gómez, J.L.; MacDonald, N.R.; Molina, S.N.; et al. Kinematics of Parsec-scale Jets of Gamma-Ray Blazars at 43 GHz within the VLBA-BU-BLAZAR Program. *Astrophys. J.* **2017**, *846*, 98. [\[CrossRef\]](#)

188. Pushkarev, A.B.; Kovalev, Y.Y.; Lister, M.L.; Savolainen, T. Jet opening angles and gamma-ray brightness of AGN*. *Astron. Astrophys.* **2009**, *507*, L33–L36. [\[CrossRef\]](#)

189. Tchekhovskoy, A.; Narayan, R.; McKinney, J.C. Efficient generation of jets from magnetically arrested accretion on a rapidly spinning black hole. *Mon. Not. R. Astron. Soc. Lett.* **2011**, *418*, L79–L83. [\[CrossRef\]](#)

190. Gammie, C.F.; McKinney, J.C.; Toth, G. HARM: A Numerical Scheme for General Relativistic Magnetohydrodynamics. *Astrophys. J.* **2003**, *589*, 444. [\[CrossRef\]](#)

191. Komissarov, S.S. General relativistic magnetohydrodynamic simulations of monopole magnetospheres of black holes. *Mon. Not. R. Astron. Soc.* **2004**, *350*, 1431–1436. [\[CrossRef\]](#)

192. Igumenshchev, I.V.; Narayan, R.; Abramowicz, M.A. Three-dimensional Magnetohydrodynamic Simulations of Radiatively Inefficient Accretion Flows. *Astrophys. J.* **2003**, *592*, 1042. [\[CrossRef\]](#)

193. McKinney, J.C. General relativistic magnetohydrodynamic simulations of the jet formation and large-scale propagation from black hole accretion systems. *Mon. Not. R. Astron. Soc.* **2006**, *368*, 1561–1582. [\[CrossRef\]](#)

194. Beckwith, K.; Hawley, J.F.; Krolik, J.H. The Influence of Magnetic Field Geometry on the Evolution of Black Hole Accretion Flows: Similar Disks, Drastically Different Jets. *Astrophys. J.* **2008**, *678*, 1180. [\[CrossRef\]](#)

195. Nealon, R.; Price, D.J.; Nixon, C.J. On the Bardeen–Petterson effect in black hole accretion discs. *Mon. Not. R. Astron. Soc.* **2015**, *448*, 1526–1540. [\[CrossRef\]](#)

196. Narayan, R.; Sadowski, A.; Penna, R.F.; Kulkarni, A.K. GRMHD simulations of magnetized advection-dominated accretion on a non-spinning black hole: Role of outflows. *Mon. Not. R. Astron. Soc.* **2012**, *426*, 3241–3259. [\[CrossRef\]](#)

197. Lalakos, A.; Gottlieb, O.; Kaaz, N.; Chatterjee, K.; Liska, M.; Christie, I.M.; Tchekhovskoy, A.; Zhuravleva, I.; Nokhrina, E. Bridging the bondi and event horizon scales: 3d grmhd simulations reveal x-shaped radio galaxy morphology. *Astrophys. J. Lett.* **2022**, *936*, L5. [\[CrossRef\]](#)

198. Igumenshchev, I.V. Magnetically Arrested Disks and the Origin of Poynting Jets: A Numerical Study. *Astrophys. J.* **2008**, *677*, 317. [\[CrossRef\]](#)

199. Dexter, J.; McKinney, J.C.; Agol, E. The size of the jet launching region in M87. *Mon. Not. R. Astron. Soc.* **2012**, *421*, 1517–1528. [\[CrossRef\]](#)

200. Yamamoto, R.; Takasao, S. Magnetic field transport in geometrically thick discs: Multidimensional effects on the field strength and inclination angle. *Mon. Not. R. Astron. Soc.* **2024**, *530*, 1218–1234. [\[CrossRef\]](#)

201. Jiang, Y.-F.; Stone, J.M.; Davis, S.W. Super-Eddington Accretion Disks around Supermassive Black Holes. *Astrophys. J.* **2019**, *880*, 67. [\[CrossRef\]](#)

202. Sadowski, A.; Narayan, R.; Penna, R.; Zhu, Y. Energy, momentum and mass outflows and feedback from thick accretion discs around rotating black holes. *Mon. Not. R. Astron. Soc.* **2013**, *436*, 3856–3874. [\[CrossRef\]](#)

203. Olivares, H.; Porth, O.; Davelaar, J.; Most, E.R.; Fromm, C.M.; Mizuno, Y.; Younsi, Z.; Rezzolla, L. Constrained transport and adaptive mesh refinement in the Black Hole Accretion Code. *Astron. Astrophys.* **2019**, *629*, A61. [\[CrossRef\]](#)

204. Porth, O.; Olivares, H.; Mizuno, Y.; Younsi, Z.; Rezzolla, L.; Moscibrodzka, M.; Falcke, H.; Kramer, M. The black hole accretion code. *Comput. Astrophys. Cosmol.* **2017**, *4*, 1. [\[CrossRef\]](#)

205. Dedner, A.; Kemm, F.; Kröner, D.; Munz, C.-D.; Schnitzer, T.; Wesenberg, M. Hyperbolic Divergence Cleaning for the MHD Equations. *J. Comput. Phys.* **2002**, *175*, P. 645–673. [\[CrossRef\]](#)

206. Tóth, G. The $\nabla \cdot \mathbf{B} = 0$ constraint in shock-capturing magnetohydrodynamics codes. *J. Comput. Phys.* **2000**, *161*, 605–652. [\[CrossRef\]](#)

207. Londrillo, P.; Zanna, L.D. High-Order Upwind Schemes for Multidimensional Magnetohydrodynamics. *Astrophys. J.* **2000**, *530*, 508. [\[CrossRef\]](#)

208. Mignone, A.; Zanni, C.; Tzeferacos, P.; van Straalen, B.; Colella, P.; Bodo, G. The PLUTO code for adaptive mesh computations in astrophysical fluid dynamics. *Astrophys. J. Suppl. Ser.* **2012**, *198*, 7. [\[CrossRef\]](#)

209. Ripperda, B.; Bacchini, F.; Porth, O.; Most, E.R.; Olivares, H.; Nathanael, A.; Rezzolla, L.; Teunissen, J.; Keppens, R. General-relativistic Resistive Magnetohydrodynamics with Robust Primitive-variable Recovery for Accretion Disk Simulations. *Astrophys. J. Suppl. Ser.* **2019**, *244*, 10. [\[CrossRef\]](#)

210. Ressler, S.M.; White, C.J.; Quataert, E.; Stone, J.M. Ab Initio Horizon-scale Simulations of Magnetically Arrested Accretion in Sagittarius A* Fed by Stellar Winds. *Astrophys. J. Lett.* **2020**, *896*, L6. [\[CrossRef\]](#)

211. Punsly, B. Spectral Diagnostics of Blazar Central Engines. I. Observational Implications. *Astrophys. J.* **1996**, *473*, 152. [\[CrossRef\]](#)

212. Punsly, B. Spectral Diagnostics of Blazar Central Engines. II. Hydromagnetic Theory. *Astrophys. J.* **1996**, *473*, 178. [\[CrossRef\]](#)

213. Punsly, B. Spectral Diagnostics of Blazar Central Engines. III. Submillimeter Flares in Blazars. *Astrophys. J.* **1997**, *474*, 612. [\[CrossRef\]](#)

214. Petropoulou, M.; Mastichiadis, A. Bethe–Heitler emission in BL Lacs: Filling the gap between X-rays and γ -rays. *Mon. Not. R. Astron. Soc.* **2015**, *447*, 36–48. [\[CrossRef\]](#)

215. Loureiro, N.F.; Samtaney, R.; Schekochihin, A.A.; Uzdensky, D.A. Magnetic reconnection and stochastic plasmoid chains in high-Lundquist-number plasmas. *Phys. Plasmas* **2012**, *19*, 042303. [\[CrossRef\]](#)

216. Guo, F.; Li, H.; Daughton, W.; Liu, Y.-H. Formation of hard power laws in the energetic particle spectra resulting from relativistic magnetic reconnection. *Phys. Rev. Lett.* **2014**, *113*, 155005. [\[CrossRef\]](#)

217. Ji, H.; Daughton, W.; Jara-Almone, J.; Le, A.; Stanier, A.; Yoo, J. Magnetic reconnection in the era of exascale computing and multiscale experiments. *Nat. Rev. Phys.* **2021**, *4*, 263–282. [\[CrossRef\]](#)

218. Yamada, M.; Kulsrud, R.; Ji, H. Magnetic reconnection. *Rev. Mod. Phys.* **2010**, *82*, 603. [\[CrossRef\]](#)

219. Hoshino, M.; Arons, J.; Gallant, Y.A.; Langdon, A.B. Relativistic magnetosonic shock waves in synchrotron sources—Shock structure and nonthermal acceleration of positrons. *Astrophys. J.* **1992**, *390*, 454. [\[CrossRef\]](#)

220. Zenitani, S.; Hoshino, M. The Generation of Nonthermal Particles in the Relativistic Magnetic Reconnection of Pair Plasmas. *Astrophys. J.* **2001**, *562*, L63. [\[CrossRef\]](#)

221. Hesse, M.; Cassak, P.A. Magnetic Reconnection in the Space Sciences: Past, Present, and Future. *J. Geophys. Res. Space Phys.* **2019**, *125*, 2. [\[CrossRef\]](#)

222. Guo, F.; Liu, Y.-H.; Daughton, W.; Li, H. Particle acceleration and plasma dynamics during magnetic reconnection in the magnetically dominated regime. *Astrophys. J.* **2015**, *806*, 167. [\[CrossRef\]](#)

223. Kagan, D.; Sironi, L.; Cerutti, B.; Giannios, D. Relativistic Magnetic Reconnection in Pair Plasmas and Its Astrophysical Applications. *Space Sci. Rev.* **2015**, *191*, 545–573. [\[CrossRef\]](#)

224. Sironi, L.; Giannios, D.; Petropoulou, M. Plasmoids in relativistic reconnection, from birth to adulthood: First they grow, then they go. *Mon. Not. R. Astron. Soc.* **2016**, *462*, 48–74. [\[CrossRef\]](#)

225. Werner, G.R.; Uzdensky, D.A.; Cerutti, B.; Nalewajko, K.; Begelman, M.C. The extent of power-law energy spectra in collisionless relativistic magnetic reconnection in pair plasmas. *Astrophys. J. Lett.* **2016**, *816*, L8. [\[CrossRef\]](#)

226. Comisso, L.; Sironi, L. Particle Acceleration in Relativistic Plasma Turbulence. *Astrophys. J.* **2018**, *121*, 255101. [\[CrossRef\]](#)

227. Alves, E.P.; Grismayer, T.; Martins, S.F.; Fiúza, F.; Fonseca, R.A.; Silva, L.O. Large-scale magnetic field generation via the kinetic Kelvin–Helmholtz instability in unmagnetized scenarios. *Astrophys. J. Lett.* **2012**, *746*, L14. [\[CrossRef\]](#)

228. Grismayer, T.; Alves, E.P.; Fonseca, R.A.; Silva, L.O. dc-Magnetic-Field Generation in Unmagnetized Shear Flows. *Phys. Rev. Lett.* **2013**, *111*, 015005. [\[CrossRef\]](#)

229. Squire, J.; Hopkins, P.F. Resonant drag instabilities in protoplanetary discs: The streaming instability and new, faster growing instabilities. *Mon. Not. R. Astron. Soc.* **2018**, *477*, 5011–5040. [\[CrossRef\]](#)

230. Martins, S.F.; Fonseca, R.A.; Silva, L.O.; Mori, W.B. Ion dynamics and acceleration in relativistic shocks. *Astrophys. J.* **2009**, *695*, L189. [\[CrossRef\]](#)

231. Spitkovsky, A. Particle Acceleration in Relativistic Collisionless Shocks: Fermi Process at Last? *Astrophys. J.* **2016**, *682*, L5. [\[CrossRef\]](#)

232. Nishikawa, K.I.; Hardee, P.; Richardson, G.; Preece, R.; Sol, H.; Fishman, G.J. Particle Acceleration in Relativistic Jets Due to Weibel Instability. *Astrophys. J.* **2003**, *595*, 555. [\[CrossRef\]](#)

233. Sironi, L.; Spitkovsky, A. Particle acceleration in relativistic magnetized collisionless electron-ion shocks. *Astrophys. J.* **2011**, *726*, 75. [\[CrossRef\]](#)

234. Caprioli, D.; Spitkovsky, A. Simulations of Ion Acceleration at Non-relativistic Shocks. I. Acceleration Efficiency. *Astrophys. J.* **2014**, *783*, 91. [\[CrossRef\]](#)

235. Park, J.; Caprioli, D.; Spitkovsky, A. Simultaneous Acceleration of Protons and Electrons at Nonrelativistic Quasiparallel Collisionless Shocks. *Phys. Rev. Lett.* **2015**, *114*, 085003. [\[CrossRef\]](#)

236. Amano, T.; Hoshino, M. Electron injection at high Mach number quasi-perpendicular shocks: Surfing and drift acceleration. *Astrophys. J.* **2007**, *661*, 190. [\[CrossRef\]](#)

237. Kunz, M.W.; Stone, J.M.; Bai, X.-N. Pegasus: A new hybrid-kinetic particle-in-cell code for astrophysical plasma dynamics. *J. Comput. Phys.* **2014**, *259*, 154–174. [\[CrossRef\]](#)

238. Comisso, L.; Sironi, L. The Interplay of Magnetically Dominated Turbulence and Magnetic Reconnection in Producing Nonthermal Particles. *Astrophys. J.* **2019**, *886*, 122. [\[CrossRef\]](#)

239. Caprioli, D. Understanding hadronic gamma-ray emission from supernova remnants. *J. Cosmol. Astropart. Phys.* **2011**, *JCAP05*, 026. [\[CrossRef\]](#)

240. Riquelme, M.A.; Spitkovsky, A. Electron Injection by Whistler Waves in Non-Relativistic Shocks. *Astrophys. J.* **2011**, *733*, 63. [\[CrossRef\]](#)

241. Liu, Y.-H.; Hesse, M.; Guo, F.; Daughton, W.; Li, H.; Cassak, P.A.; Shay, M.A. Why does Steady-State Magnetic Reconnection have a Maximum Local Rate of Order 0.1? *Phys. Rev. Lett.* **2017**, *118*, 085101. [\[CrossRef\]](#) [\[PubMed\]](#)

242. Bessho, N.; Chen, L.; Shuster, J.R.; Wang, S. Electron distribution functions in the electron diffusion region of magnetic reconnection: Physics behind the fine structures. *Geophys. Res. Lett.* **2014**, *41*, 8688–8695. [\[CrossRef\]](#)

243. MacDonald, N.R.; Marscher, A.P.; Jorstad, S.G.; Joshi, M. Through the Ring of Fire: Gamma-Ray Variability in Blazars by a Moving Plasmoid Passing a Local Source of Seed Photons. *Astrophys. J.* **2015**, *804*, 111. [\[CrossRef\]](#)

244. Wardle, J. The variable rotation measure distribution in 3C 273 on parsec scales. *Galaxies* **2018**, *6*, 5. [\[CrossRef\]](#)

245. Gold, R.; Broderick, A.E.; Younsi, Z.; Fromm, C.M.; Gammie, C.F.; Mościbrodzka, M.; Pu, H.-Y.; Bronzwaer, T.; Davelaar, J.; Dexter, J.; et al. Verification of Radiative Transfer Schemes for the EHT. *Astrophys. J.* **2020**, *897*, 148. [\[CrossRef\]](#)

246. Mościbrodzka, M.; Gammie, C.F.; Dolence, J.C.; Shiokawa, H.; Leung, P.K. Radiative models of SGR A* from GRMHD simulations. *Astrophys. J.* **2009**, *706*, 497. [\[CrossRef\]](#)

247. Acharyya, A. Multiwavelength Observations of the Blazar PKS 0735+178 in Spatial and Temporal Coincidence with an Astrophysical Neutrino Candidate IceCube-211208A. *arXiv* **2023**, arXiv:2306.17819. [\[CrossRef\]](#)

248. Dolence, J.C.; Gammie, C.F.; Mościbrodzka, M.; Leung, P.K. grmonty: A Monte Carlo code for relativistic radiative transport. *Astrophys. J. Suppl. Ser.* **2009**, *184*, 387. [\[CrossRef\]](#)

249. Noble, S.C.; Gammie, C.F.; McKinney, J.C.; Del Zanna, L. Primitive Variable Solvers for Conservative General Relativistic Magnetohydrodynamics. *Astrophys. J.* **2006**, *641*, 626. [\[CrossRef\]](#)

250. Shcherbakov, R.V.; Penna, R.F.; McKinney, J.C. Sagittarius A* accretion flow and black hole parameters from general relativistic dynamical and polarized radiative modeling. *Astrophys. J.* **2012**, *755*, 133. [\[CrossRef\]](#)

251. Broderick, A.E.; Loeb, A.; Narayan, R. The Event Horizon of Sagittarius A*. *Astrophys. J.* **2009**, *701*, 1357. [\[CrossRef\]](#)

252. Rybicki, G.B.; Lightman, A.P. *Radiative Processes in Astrophysics*; John Wiley & Sons: Hoboken, NJ, USA, 2024; p. 400.

253. Jones, T.W.; O'Dell, S.L.; Stein, W.A. Physics of Compact Nonthermal Sources. I. Theory of Radiation Processes. *Astrophys. J.* **1974**, *188*, 353–368. [\[CrossRef\]](#)

254. Marscher, A.P.; Gear, W.K. Models for high-frequency radio outbursts in extragalactic sources, with application to the early 1983 millimeter-to-infrared flare of 3C 273. *Astrophys. J.* **1985**, *298*, 114–127. [\[CrossRef\]](#)

255. Dermer, C.D.; Reinhard, S. Model for the High-Energy Emission from Blazars. *Astrophys. J.* **1993**, *416*, 458. [\[CrossRef\]](#)

256. Sikora, M.; Begelman, M.C.; Rees, M.J. Comptonization of diffuse ambient radiation by a relativistic jet: The source of gamma rays from blazars? *Astrophys. J.* **1994**, *421*, 153. [\[CrossRef\]](#)

257. Finke, J.D. External Compton scattering in blazar jets and the location of the gamma-ray emitting region. *Astrophys. J.* **2016**, *830*, 94. [\[CrossRef\]](#)

258. Nalewajko, K.; Zrake, J.; Yuan, Y.; East, W.E.; Blandford, R.D. Kinetic simulations of the lowest-order unstable mode of relativistic magnetostatic equilibria. *Astrophys. J.* **2016**, *826*, 115. [\[CrossRef\]](#)

259. Mannheim, K. The proton blazar. *Astron. Astrophys.* **1993**, *269*, 67–76.

260. Atoyan, A.M.; Dermer, C.D. Neutral beams from blazar jets. *Astron. Astrophys.* **2003**, *586*, 79. [\[CrossRef\]](#)

261. Mashchenko, S. Modelling the light curve of 'Oumuamua: Evidence for torque and disc-like shape. *Mon. Not. R. Astron. Soc.* **2019**, *489*, 3003–3021. [\[CrossRef\]](#)

262. Celotti, A.; Ghisellini, G. The power of blazar jets. *Mon. Not. R. Astron. Soc.* **2008**, *385*, 283–300. [\[CrossRef\]](#)

263. Finke, J.D. The Compton dominance and the blazar sequence. *Astrophys. J.* **2013**, *763*, 134. [\[CrossRef\]](#)

264. Moderski, R.; Sikora, M.; Coppi, P.S.; Aharonian, F. Klein–Nishina effects in the spectra of non-thermal sources immersed in external radiation fields. *Mon. Not. R. Astron. Soc.* **2005**, *363*, 954–966. [\[CrossRef\]](#)

265. Webb, J.R. Multi-Frequency Blazar Micro-Variability as a Tool to Investigate Relativistic Jets. *Galaxies* **2016**, *4*, 15. [\[CrossRef\]](#)

266. Tahani, K.; Plume, R.; Bergin, E.A.; Tolls, V.; Phillips, T.G.; Caux, E.; Cabrit, S.; Goicoechea, J.R.; Goldsmith, P.F.; Johnstone, D.; et al. Analysis of the Herschel/Hexos Spectral Survey Toward Orion South: A Massive Protostellar Envelope with Strong External Irradiation. *Astrophys. J.* **2016**, *832*, 12. [\[CrossRef\]](#)

267. Levermore, C.D. Relating Eddington factors to flux limiters. *J. Quant. Spectrosc. Radiat. Transf.* **1984**, *31*, 149–160. [\[CrossRef\]](#)

268. Sadowski, A.; Wielgus, M.; Narayan, R.; Abarca, D.; McKinney, J.C.; Chael, A. Radiative, two-temperature simulations of low-luminosity black hole accretion flows in general relativity. *Mon. Not. R. Astron. Soc.* **2017**, *466*, 705–725. [\[CrossRef\]](#)

269. Jiang, Y.-F.; Stone, J.M.; Davis, S.W. A Godunov method for multidimensional radiation magnetohydrodynamics based on a variable Eddington tensor. *Astrophys. J. Suppl. Ser.* **2012**, *199*, 14. [\[CrossRef\]](#)

270. Sadowski, A.; Lasota, J.-P.; Abramowicz, M.A.; Narayan, R. Energy flows in thick accretion discs and their consequences for black hole feedback. *Mon. Not. R. Astron. Soc.* **2016**, *456*, 3915–3928. [\[CrossRef\]](#)

271. Carleo, G.; Cirac, I.; Cranmer, K.; Daudet, L.; Schuld, M.; Tishby, N.; Vogt-Maranto, L.; Zdeborová, L. Machine learning and the physical sciences. *Rev. Mod. Phys.* **2019**, *91*, 045002. [\[CrossRef\]](#)

272. Cranmer, K.; Brehmer, J.; Louppe, G. The frontier of simulation-based inference. *Proc. Natl. Acad. Sci. USA* **2020**, *117*, 30055–30062. [\[CrossRef\]](#) [\[PubMed\]](#)

273. Ntampaka, M.; Avestruz, C.; Boada, S.; Caldeira, J.; Cisewski-Kehe, J.; Di Stefano, R.; Dvorkin, C.; Evrard, A.E.; Farahi, A.; Finkbeiner, D.; et al. The Role of Machine Learning in the Next Decade of Cosmology. *arXiv* **2019**, arXiv:1902.10159.

274. McNamara, B.R.; Nulsen, P.E.J. Heating Hot Atmospheres with Active Galactic Nuclei. *Annu. Rev. Astron. Astrophys.* **2007**, *45*, 117–175. [\[CrossRef\]](#)

275. Gaibler, V.; Khochfar, S.; Krause, M.; Silk, J. Jet-induced star formation in gas-rich galaxies. *Mon. Not. R. Astron. Soc.* **2012**, *425*, 438–449. [\[CrossRef\]](#)

276. Mukherjee, D.; Bicknell, G.V.; Sutherl, R.; Wagner, A. Relativistic jet feedback in high-redshift galaxies—I. Dynamics. *Mon. Not. R. Astron. Soc.* **2016**, *461*, 967–983. [\[CrossRef\]](#)

277. Clarke, D.A.; Norman, M.L.; Burns, J.O. Numerical Simulations of a Magnetically Confined Jet. *Astrophys. J.* **1986**, *311*, L63–L67. [\[CrossRef\]](#)

278. Norman, M.L.; Winkler, K.H.; Smarr, L.; Smith, M.D. Structure and dynamics of supersonic jets. *Astron. Astrophys.* **1982**, *113*, 285–302.

279. Begelman, M.C.; Blandford, R.D.; Rees, M.J. Theory of extragalactic radio sources. *Phys. Rev. J.* **1984**, *56*, 255. [\[CrossRef\]](#)

280. Kaiser, C.R. The environments and ages of extragalactic radio sources inferred from multi-frequency radio maps. *arXiv* **2000**, arXiv:astro-ph/0007261. [\[CrossRef\]](#)

281. Krause, M. Very light jets—I. Axisymmetric parameter study and analytic approximation. *Astron. Astrophys.* **2003**, *398*, 113–125. [\[CrossRef\]](#)

282. Weinberger, R.; Springel, V.; Hernquist, L.; Pillepich, A.; Marinacci, F.; Pakmor, R.; Nelson, D.; Genel, S.; Vogelsberger, M.; Naiman, J.; et al. Simulating galaxy formation with black hole driven thermal and kinetic feedback. *Mon. Not. R. Astron. Soc.* **2017**, *465*, 3291–3308. [\[CrossRef\]](#)

283. Dong, C.; Wiliardy, A.; Nagamine, K.; Oku, Y.; Oh, B.K.; Cen, R. AGN jet evolution simulation with GADGET4-OSAKA. *arXiv* **2025**, arXiv:2508.21282. [\[CrossRef\]](#)

284. Birkinshaw, M. *Beams and Jets in Astrophysics: The Stability of Jets*; Cambridge University Press: Cambridge, UK, 1991; p. 278.

285. Perucho, M.; Martí, J.M.; Cela, J.M.; Hanasz, M.; de la Cruz, R.; Rubio, F. Stability of three-dimensional relativistic jets: Implications for jet collimation. *Astron. Astrophys.* **2010**, *519*, A41. [\[CrossRef\]](#)

286. Meliani, Z.; Keppens, R. Decelerating relativistic two-component jets. *Astrophys. J.* **2009**, *705*, 1594. [\[CrossRef\]](#)

287. Rossi, P.; Mignone, A.; Bodo, G.; Massaglia, S.; Ferrari, A. Formation of dynamical structures in relativistic jets: The FRI case. *Astron. Astrophys.* **2008**, *488*, 795–806. [\[CrossRef\]](#)

288. Hardee, P.E. On Three-dimensional Structures in Relativistic Hydrodynamic Jets. *Astrophys. J.* **2000**, *533*, 176. [\[CrossRef\]](#)

289. Mizuno, Y.; Lyubarsky, Y.; Nishikawa, K.-I.; Hardee, P.E. Three-dimensional relativistic magnetohydrodynamic simulations of current-driven instability. I. Instability of a static column. *Astrophys. J.* **2009**, *700*, 684. [\[CrossRef\]](#)

290. Appl, S.; Lery, T.; Baty, H. Current-driven instabilities in astrophysical jets. Linear analysis. *Astron. Astrophys.* **2000**, *355*, 818–828.

291. Mizuno, Y.; Pohl, M.; Niemiec, J.; Zhang, B.; Nishikawa, K.-I.; Hardee, P.E. Magnetic field amplification and saturation in turbulence behind a relativistic shock. *Mon. Not. R. Astron. Soc.* **2014**, *439*, 3490–3503. [\[CrossRef\]](#)

292. Li, H.; Lapenta, G.; Finn, J.M.; Li, S.; Colgate, S.A. Modeling the Large-Scale Structures of Astrophysical Jets in the Magnetically Dominated Limit. *Astrophys. J.* **2006**, *643*, 92. [\[CrossRef\]](#)

293. O'Neill, S.M.; Beckwith, K.; Begelman, M.C. Local simulations of instabilities in relativistic jets—I. Morphology and energetics of the current-driven instability. *Mon. Not. R. Astron. Soc.* **2012**, *422*, 1436–1452. [\[CrossRef\]](#)

294. Nakamura, M.; Li, H.; Li, S. Stability Properties of Magnetic Tower Jets. *Astrophys. J.* **2007**, *656*, 721. [\[CrossRef\]](#)

295. Singh, C.B.; Mizuno, Y.; Pino, E.M.d.G.D. Spatial growth of current-driven instability in relativistic rotating jets and the search for magnetic reconnection. *Astrophys. J.* **2016**, *824*, 48. [\[CrossRef\]](#)

296. Lyutikov, M. Magnetocentrifugal launching of jets from discs around Kerr black holes. *Mon. Not. R. Astron. Soc.* **2009**, *461*, 1545–1552. [\[CrossRef\]](#)

297. Wagner, A.Y.; Bicknell, G.V.; Umemura, M. Driving outflows with relativistic jets and the dependence of active galactic nucleus feedback efficiency on interstellar medium inhomogeneity. *Astrophys. J.* **2012**, *757*, 136. [\[CrossRef\]](#)

298. King, A. Black holes, galaxy formation, and the $M_{BH}\sigma$ relation. *Astrophys. J.* **2003**, *596*, L27. [\[CrossRef\]](#)

299. Silk, J.; Rees, M.J. Quasars and galaxy formation. *Astron. Astrophys.* **1998**, *331*, L1–L4.

300. Sijacki, D.; Springel, V.; Di Matteo, T.; Hernquist, L. A unified model for AGN feedback in cosmological simulations of structure formation. *Mon. Not. R. Astron. Soc.* **2007**, *380*, 877–900. [\[CrossRef\]](#)

301. Bourne, M.A.; Sijacki, D. AGN jet feedback on a moving mesh: Cocoon inflation, gas flows and turbulence. *Mon. Not. R. Astron. Soc.* **2017**, *472*, 4707–4735. [\[CrossRef\]](#)

302. Fragile, P.C.; Murray, S.D.; Lin, D.N.C. Ejection of Supernova-enriched Gas from Dwarf Disk Galaxies. *Astrophys. J.* **2004**, *617*, 1077. [\[CrossRef\]](#)

303. Pfrommer, C.; Pakmor, R.; Schaal, K.; Simpson, C.M.; Springel, V. Simulating cosmic ray physics on a moving mesh. *Mon. Not. R. Astron. Soc.* **2017**, *465*, 4500–4529. [\[CrossRef\]](#)

304. Ruszkowski, M.; Yang, H.-Y.K.; Zweibel, E. Global simulations of galactic winds including cosmic-ray streaming. *Astrophys. J.* **2017**, *834*, 208. [\[CrossRef\]](#)

305. Barniol Duran, R.; Bošnjak, Ž.; Kumar, P. Inverse-Compton cooling in Klein-Nishina regime and gamma-ray burst prompt spectrum. *Mon. Not. R. Astron. Soc.* **2012**, *424*, 3192–3200. [\[CrossRef\]](#)

306. Pfrommer, C.; Springel, V.; Ensslin, T.A.; Jubelgas, M. Detecting shock waves in cosmological smoothed particle hydrodynamics simulations. *Mon. Not. R. Astron. Soc.* **2006**, *367*, 113–131. [\[CrossRef\]](#)

307. Guo, F.; Oh, S.P. Feedback heating by cosmic rays in clusters of galaxies. *Mon. Not. R. Astron. Soc.* **2008**, *384*, 251–266. [\[CrossRef\]](#)

308. Salem, M.; Bryan, G.L.; Hummels, C. Cosmological Simulations of Galaxy Formation with Cosmic Rays. *Astrophys. J. Lett.* **2014**, *797*, L18.

309. Sikora, M.; Begelman, M.C.; Madejski, G.M.; Lasota, J.P. Are Quasar Jets Dominated by Poynting Flux? *Astrophys. J.* **2005**, *625*, 72. [\[CrossRef\]](#)

310. Homan, D.C.; Kovalev, Y.Y.; Lister, M.L.; Ros, E.; Kellermann, K.I.; Cohen, M.H.; Vermeulen, R.C.; Zensus, J.A.; Kadler, M. Intrinsic Brightness Temperatures of AGN Jets. *Astrophys. J.* **2006**, *642*, L115. [\[CrossRef\]](#)

311. Jones, T.W.; De Young, D.S. Magnetohydrodynamic Simulations of Relic Radio Bubbles in Clusters. *Astrophys. J.* **2005**, *624*, 586. [\[CrossRef\]](#)

312. Broderick, A.E.; McKinney, J.C. Parsec-Scale Faraday Rotation Measures from General Relativistic Magnetohydrodynamic Simulations of Active Galactic Nucleus Jets. *Astrophys. J.* **2010**, *725*, 750. [\[CrossRef\]](#)

313. Lyutikov, M.; Pariev, V.I.; Gabuzda, D.C. Polarization and structure of relativistic parsec-scale AGN jets. *Mon. Not. R. Astron. Soc.* **2005**, *360*, 869–891. [\[CrossRef\]](#)

314. Donea, A.C.; Protheroe, R.J. Radiation fields of disk, BLR and torus in quasars and blazars: Implications for gamma-ray absorption. *Astropart. Phys.* **2003**, *18*, 377–393. [\[CrossRef\]](#)

315. Gould, R.J.; Schréder, G.P. Pair Production in Photon-Photon Collisions. *Phys. Rev.* **1967**, *155*, 1404. [\[CrossRef\]](#)

316. Kirk, J.G.; Guthmann, A.W.; Gallant, Y.A.; Achterberg, A. Particle Acceleration at Ultrarelativistic Shocks: An Eigenfunction Method. *Astrophys. J.* **2000**, *542*, 235. [\[CrossRef\]](#)

317. Lemoine, M.; Li, Z.; Wang, X.-Y. On the magnetization of gamma-ray burst blast waves. *Mon. Not. R. Astron. Soc.* **2013**, *435*, 3009–3016. [\[CrossRef\]](#)

318. Bell, A.R. The acceleration of cosmic rays in shock fronts—I. *Mon. Not. R. Astron. Soc.* **1978**, *182*, 147–156. [\[CrossRef\]](#)

319. Blandford, R.D.; Ostriker, J.P. Particle acceleration by astrophysical shocks. *Astrophys. J.* **1978**, *221*, L29–L32. [\[CrossRef\]](#)

320. Cerutti, B.; Werner, G.R.; Uzdensky, D.A.; Begelman, M.C. Three-Dimensional Relativistic Pair Plasma Reconnection with Radiative Feedback in the Crab Nebula. *Astrophys. J.* **2014**, *782*, 104. [\[CrossRef\]](#)

321. Uzdensky, D.A.; Loureiro, N.F.; Schekochihin, A.A. Fast magnetic reconnection in the plasmoid-dominated regime. *Phys. Rev. Lett.* **2010**, *105*, 235002. [\[CrossRef\]](#) [\[PubMed\]](#)

322. Schlickeiser, R. *Cosmic Ray Astrophysics*, 1st ed.; Springer: Berlin/Heidelberg, Germany; New York, NY, USA, 2002; p. 519.

323. Loureiro, N.F.; Boldyrev, S. Role of Magnetic Reconnection in Magnetohydrodynamic Turbulence. *Phys. Rev. Lett.* **2017**, *118*, 245101. [\[CrossRef\]](#) [\[PubMed\]](#)

324. Lemoine, M. Generalized Fermi acceleration. *Phys. Rev. D* **2019**, *99*, 083006. [\[CrossRef\]](#)

325. Sebastian, S.T.; Comisso, L. Magnetic Field-line Curvature and Its Role in Particle Acceleration by Magnetically Dominated Turbulence. *Astrophys. J. Lett.* **2025**, *994*, L1. [\[CrossRef\]](#)

326. Das, S.; Xu, S.; Nättilä, J. Studying mirror acceleration via kinetic simulations of relativistic plasma turbulence. *arXiv* **2025**, arXiv:2506.04212. [\[CrossRef\]](#)

327. Tanner, R.; Weaver, K.A. Simulations of AGN-driven Galactic Outflow Morphology and Content. *Astron. J.* **2022**, *163*, 134. [\[CrossRef\]](#)

328. Lynden-Bell, D. Magnetic collimation by accretion discs of quasars and stars. *Mon. Not. R. Astron. Soc.* **1996**, *279*, 389–401. [\[CrossRef\]](#)

329. Spruit, H. Theory of Magnetically Powered Jets. *Astrophys. J.* **2010**, *794*, 233–263.

330. Mimica, P.; Aloy, M.-A.; Agudo, I.; Martí, J.M.; Gómez, J.L.; Miralles, J.A. Spectral evolution of superluminal components in parsec-scale jets. *Astrophys. J.* **2009**, *696*, 1142. [\[CrossRef\]](#)

331. Reynolds, C.S. Observational Constraints on Black Hole Spin. *Annu. Rev. Astron. Astrophys.* **2021**, *59*, 117–154. [\[CrossRef\]](#)

332. Morabito, L.K.; Williams, W.L.; Duncan, K.J.; Röttgering, H.J.A.; Miley, G.; Saxena, A.; Barthel, P.; Best, P.N.; Bruggen, M.; Brunetti, G.; et al. Investigating the unification of LOFAR-detected powerful AGN in the Boötes field. *Mon. Not. R. Astron. Soc.* **2017**, *469*, 1883–1896. [\[CrossRef\]](#)

333. Alves, B.R.; Biteau, J.; Bustamante, M.; Dolag, K.; Engel, R.; Fang, K.; Kampert, K.H.; Kostunin, D.; Mostafa, M.; Murase, K.; et al. Open questions in cosmic-ray research at ultrahigh energies. *Front. Astron. Space Sci.* **2019**, *6*, 23. [\[CrossRef\]](#)

334. Kotera, K.; Allard, D.; Olinto, A. Cosmogenic neutrinos: Parameter space and detectability from PeV to ZeV. *J. Cosmol. Astropart. Phys.* **2010**, *2010*, 013. [\[CrossRef\]](#)

335. Bell, A.R.; Schure, K.M.; Reville, B.; Giacinti, G. Cosmic-ray acceleration and escape from supernova remnants. *Mon. Not. R. Astron. Soc.* **2013**, *431*, 415–429. [\[CrossRef\]](#)

336. Murase, K.; Dermer, C.D.; Takami, H.; Migliori, G. Blazars as ultra-high-energy cosmic-ray sources: Implications for TeV gamma-ray observations. *Astrophys. J.* **2012**, *749*, 63. [\[CrossRef\]](#)

337. Aartsen, M.G.; Abbasi, R.; Ackermann, M.; Adams, J.; A Aguilar, J.; Ahlers, M.; Ahrens, M.; Alispach, C.; Allison, P.; Amin, N.M.; et al. IceCube-Gen2: The window to the extreme Universe. *J. Phys. G Nucl. Part. Phys.* **2021**, *48*, 060501. [\[CrossRef\]](#)

338. LHAASO Collaboration. A tera-electron volt afterglow from a narrow jet in an extremely bright gamma-ray burst. *Science* **2023**, *380*, 1390–1396. [\[CrossRef\]](#)

339. Burns, E. GRB 221009A: The BOAT. *Astrophys. J. Lett.* **2023**, *946*, L31. [\[CrossRef\]](#)

340. IceCube Collaboration. Evidence for neutrino emission from the nearby active galaxy NGC 1068. *Science* **2022**, *378*, 538–543. [\[CrossRef\]](#)

341. Telescope Array Collaboration. An extremely energetic cosmic ray observed by a surface detector array. *Science* **2023**, *382*, 903–907. [\[CrossRef\]](#)

342. Das, S.; Hazra, S.; Gupta, N. Cosmic Clues from Amaterasu: Blazar-driven Ultrahigh-energy Cosmic Rays? *Astrophys. J. Lett.* **2025**, *988*, L8. [\[CrossRef\]](#)

343. Anchordoqui, L.A. Ultra-high-energy cosmic rays. *Phys. Rep.* **2019**, *801*, 1–93. [\[CrossRef\]](#)

344. Abbott, B.P.; Abbott, R.; Abbott, T.D.; Abernathy, M.R.; Acernese, F.; Ackley, K.; Adams, C.; Adams, T.; Addesso, P.; Adhikari, R.X.; et al. Observation of gravitational waves from a binary black hole merger. *Phys. Rev. Lett.* **2016**, *116*, 061102. [\[CrossRef\]](#) [\[PubMed\]](#)

345. Ghirlanda, G.; Salafia, O.S.; Paragi, Z.; Giroletti, M.; Yang, J.; Marcote, B.; Blanchard, J.; Agudo, I.; An, T.; Bernardini, M.G.; et al. Compact radio emission indicates a structured jet was produced by a binary neutron star merger. *Science* **2019**, *363*, 968–971. [\[CrossRef\]](#)

346. Reitze, D.; Adhikari, R.X.; Ballmer, S.; Barish, B.; Barsotti, L.; Billingsley, G.; Brown, D.A.; Chen, Y.; Coyne, D.; Eisenstein, R.; et al. Cosmic Explorer: The U.S. Contribution to Gravitational-Wave Astronomy beyond LIGO. *arXiv* **2019**, arXiv:1907.04833.

347. Porth, O.; Chatterjee, K.; Narayan, R.; Gammie, C.F.; Mizuno, Y.; Anninos, P.; Baker, J.G.; Bugli, M.; Chan, C.-K.; Davelaar, J.; et al. The Event Horizon General Relativistic Magnetohydrodynamic Code Comparison Project. *Astrophys. J. Suppl. Ser.* **2019**, *243*, 26. [\[CrossRef\]](#)

Disclaimer/Publisher’s Note: The statements, opinions and data contained in all publications are solely those of the individual author(s) and contributor(s) and not of MDPI and/or the editor(s). MDPI and/or the editor(s) disclaim responsibility for any injury to people or property resulting from any ideas, methods, instructions or products referred to in the content.